Alma Mater Studiorum · Università di Bologna

SCHOOL OF ENGINEERING

- Forlí Campus -

Master's Degree in Aerospace Engineering

class LM20

Graduation Thesis in:

Experimental Methods in Aerodynamics

Numerical modeling of a hot-wire anemometer in turbulent flows

Candidate :
Lorenzo Lazzarini

Supervisor :
Prof. Gabriele Bellani

Co-Supervisors :
Prof. Ramis Örlü
Prof. Philipp Schlatter
Prof. Alessandro Talamelli

Session III
Academic Year 2017/2018

Abstract

The present thesis deals with the numerical modeling of an hot wire anemometer inside a turbulent channel flow at $Re_\tau = 180$ with heat transfer. There are two main approaches when studying turbulence: one could follow an experimental path or a numerical approach could be pursued. Experiments showed some issues when measuring turbulence with hot wire anemometry, spatial and temporal filtering are two examples of such problems. In the present work, numerical simulations were performed in order to validate a code that model a hot-wire probe inside a turbulent channel flow. Direct Numerical Simulation (DNS) solved through a spectral code were used to build such model, due to their high level of precision and resolution. A validation process was performed starting from Kim & Moin[9] experience and Kasagi studies[7] related to DNS of channel flow with passive scalar. Following this path we implement inside our code a line source of heat mimicking the hot-wire behaviour. While simulations were running we collected statistics in order to know the values regarding turbulence fluctuations throughout the entire channel. We obtained a new data-set coming from DNS and spectral element method with not only just a passive scalar but a precise implementation of an hot-wire probe.

Key words: Wall turbulence, CFD, Direct Numerical Simulation, Spectral Method, Statistics, Hot-wire, Constant Current Anemometer.

Contents

List of Figures

Chapter 1

Introduction

Many phenomena commonly observed everyday are turbulent flows: the smoke rising from a fire or the wake of a boat. Turbulence appears as a chaotic process characterized by eddies of different size and intensity that evolve and interact with each other. Nature gives us examples of the so-called free turbulent flows, like wakes or jets, but many are the everyday situations where turbulent flows interacts with surfaces, like pipelines, air flowing over a car or a wing. The desire to gain knowledge of such complex phenomenon is not only motivated by the desire of a deeper physical understanding of the problem; turbulence is present in many industrial field such as ground transportation, energy production and climate prediction. Gain a better understand on the phenomenon can lead to great improvements in the efficiency of this industrial and environmental applications as well as the development of better models to simulate and predict turbulent flows.

In order to shed light on one of the last unresolved problems of classical physics, two main approaches are widely used to access turbulence informations: experiments or numerical simulations. Osborne Reynolds[14] was the first to carry out a systematic study on turbulence, while Kim, Moin and Moser in 1987 were the first in developing a direct numerical simulation of a turbulent channel flow. Both experimental study and numerical simulations have their advantage and disadvantage that need to be known in order to choose the best option for the considered case. Numerical simulations have

become an affordable method only in the last decades due to the increasing in computer performances. Thanks to this, Direct Numerical Simulations (DNS) can access Reynolds number of practical interest; in this approach Navier-Stokes equations are fully resolved up to the smallest scales of space and time, allowing the characterization of scales so far too small to be captured by experimental sensors.

The need for numerical simulations results as Moin suggested [10] can be also related to some problems in experimental studies. In turbulence, as the Reynolds number increase, the size of the smallest scales become smaller and smaller thus when performing an experimental study we are not able to capture this small features. Hot wire anemometry is one of the most used sensor to access information of near wall structures. However it has a fixed size and it is not able to fully capture them, this phenomenon is called spatial averaging. Örlü [11] and Hutchins [5] pointed out these issues respectively in spatial and temporal filtering during hot wire measurements. This problem represents one of the open question in experimental studies, as well as the interaction of the heat with the wall.

The aim of the present thesis is therefore the development of a new numerical code to understand and study problems related to hot wire measurement. Spectral method represents a high order numerical scheme that efficiently allow us to solve direct numerical simulations up to the smallest turbulence scales. The use of such high level numerical codes brings limitation in terms of computational cost, domain complexity and boundary condition limitations. One of the most challenging process is represented by the introduction of non linear and finite term, as an hot wire could be, in a code structured for simple geometry, mainly duct, and periodic boundary conditions.

The present thesis is structured as follows: the second chapter defines mathematical tools and theoretical concept needed to better understand wall bounded flows in general and channel flow in particular since this is the case we will deal with in the context of this thesis. Chapter 3 explains how hot-wire anemometer works and which problems are faced in experiments. Throughout the fourth chapter all the numerical schemes are exploited, giving an overview to the spectral element method and why it is useful in the

context of the current work, moreover the set up of the simulation will be defined. Chapter 5 regards the methodology and the validation process carried out to confirm the goodness of the considered test case. Chapter 6 shows the results obtained simulating the complete case. Finally in chapter 7 the conclusion coupled with future possibilities are summarized.

Chapter 2

Theoretical background

In this chapter some basic concepts related to turbulence and fluid dynamics that will help the reader throughout the thesis will be given.

2.1 Turbulence

There are many phenomena commonly observed in everyday life that are turbulent: one could be the smoke exiting from a chimney, the wake of a boat or the motion of clouds on a windy day. We can clearly see, observing for example a waterfall, that a turbulent flow is unsteady, irregular, and of course, the movement of every eddy or droplet is unpredictable. An essential feature of turbulent flows is that the velocity field varies significantly in both space and time.

Considering some engineering applications, turbulent flows are quite common: flows around vehicles such as airplanes, submarines or automobiles are generally turbulent. An important characteristic of turbulence is its ability to transport and mix fluids more efficient than its laminar counterpart; this "mixing" ability, if we consider the momentum of the flow will cause the rise of shear stresses (i.e. the drag) much more when compared to a laminar flow.

All the features mentioned above are the main motivation for studying a turbulent flow; remebering also that heat transfer in flows is of great practical importance. [13]

2.2 Governing equation

The set of equations that govern the fluid motions are the Navier-Stokes equations. Before introducing them, the *Continuum Hypothesis*, should be mentioned, where at sufficent small scales, a finite number of molecules could be interpreted in a continuum view.

2.2.1 Continuity equation

The *Mass-Conservation* or *Continuity* equation is:

$$\frac{\partial \rho}{\partial t} + \rho \nabla \cdot \overline{U} = 0. \tag{2.1}$$

where t represents the time, ρ the density of the considered fluid and U is the velocity vector; If we are dealing with incompressible flows, thus $\rho = const.$, equation (2.1) reduces to

$$\frac{\partial u_i}{\partial x_i} = 0. \tag{2.2}$$

2.2.2 Momentum equation

The momentum equation, based on Newton's second law, relates the fluid particles acceleration with body and external forces experieced by the fluid:

$$F = m\frac{d\overline{U}}{dt}. \tag{2.3}$$

Where m represents the mass, and dU/dt is the acceleration. The right-hand side of equation (2.3) can be manipulated considering a material volume $V(t)$, the Reynolds transport theorem and the Continuity equation:

$$\frac{D}{Dt}\int_{V(t)} \rho\overline{U}dV = \int_V \frac{D(\rho\overline{U})}{Dt} + \rho\overline{U}\nabla\cdot(\overline{U})dV = [..] = \int_V \rho\frac{D\overline{U}}{Dt}dV, \tag{2.4}$$

passing now on the left-hand side of relation (2.2), $\overline{F}$ can be divided in body forces $\mathbf{f}$ and tangential forces $\mathbf{t}$ as follows:

$$\overline{F} = \int_V \rho \mathbf{f} dV + \int_S \mathbf{t} dS. \tag{2.5}$$

After some mathematical manipulation we will end with momentum conservation:

$$\overline{F} = \int_V (\rho \mathbf{f} - \nabla p + \mu \nabla^2 \overline{U}) dV. \tag{2.6}$$

where p represents the pressure and μ is the dynamic viscosity. Plugging equation (2.5) inside (2.2) we will obtain:

$$\frac{D\overline{U}}{Dt} = \mathbf{f} - \frac{\nabla p}{\rho} + \nu \nabla^2 \overline{U}. \tag{2.7}$$

Equation (2.7) represents the momentum conservation, ν is the kinematic viscosity. Moreover, for a better comprehension of the successive topics we will introduce the non-dimensionalized incompressible Navier-Stokes equations in a rotating reference frame:

$$\frac{\partial u_i}{\partial t} = \frac{\partial p}{\partial x_i} + \epsilon_{ijk} u_j (\omega_k + 2\Omega_k) - \frac{\partial}{\partial x_i}\left(\frac{1}{2} u_i u_j\right) + \frac{1}{Re}\nabla^2 u_i + \mathbf{F}_i. \tag{2.8}$$

$\mathbf{F}_i$ Represents a Forcing term; Moreover, For a numerical purpose, we can rewrite momentum and continuity equation as a system of two second order equations:

$$\begin{aligned} \frac{\partial \psi}{\partial t} &= h_v + \frac{1}{Re}\nabla^2 \psi, \\ \nabla^2 v &= \psi. \end{aligned} \tag{2.9}$$

Also, taking the curl of the momentum equation (2.2), we will obtain a formulation for the normal vorticity, which, showing the second component reads:

$$\frac{\partial \omega}{\partial t} = h_\omega + \frac{1}{Re}\nabla^2 \omega, \tag{2.10}$$

where h_v and h_w are the non-linear terms; ψ, v and w are the unknown of the equations (2.9) and (2.10); since they have a similar form, they could be

solved using the same numerical routine.

2.2.3 Energy equation

As for the momentum equation, the same manipulation can be performed to obtain the energy equation; the variation of energy of any material volume is equal to the work done by external forces and the heat injected into the material volume; starting from:

$$\int_{V(t)} \rho \frac{d}{dt}(e + \frac{\overline{U}^2}{2})dV = \int_{V(t)} \rho \mathbf{f} \cdot \overline{U} dV + \int_{S(t)} (\mathbf{t} \cdot \overline{U})dS - \int_{S(t)} \mathbf{q} \cdot \mathbf{n} dS, \quad (2.11)$$

where $\mathbf{q}$ represents the heat, e the internal energy and n is the unity vector normal to the external surface S; considering again the same mathematical manipulation used for the momentum consideration we will end up with:

$$\rho \frac{d}{dt}(e + \frac{\overline{U}^2}{2}) = \rho \mathbf{f} \cdot \overline{U} + \nabla \cdot (\mathbf{T} \cdot \mathbf{V}) - \nabla \cdot q. \quad (2.12)$$

Eq. (2.12) represent the energy equation.

2.2.4 Scalar equation

In addition to the velocity $\overline{U}(x,t)$, we can consider a *conserved passive scalar* which can be denoted as $\phi(x,t)$. If we consider a constant property flow, the conservation equation for ϕ is:

$$\frac{D\phi}{Dt} = \Gamma \nabla^2 \phi, \quad (2.13)$$

where Γ is the diffusivity. The scalar ϕ is conserved, because in equation (2.9) there is no source or sink term; and it is also *passive* because by assumption its value has no effect on material properties such as ρ, ν and the velocity field. The scalar ϕ could represent different physical properties: it can be a small excess of temperature; in this case Γ will be the thermal diffusivity and ν/Γ would be the Prandtl number, Pr.

2.3 Statistical tools

In order to understand and study such a chaotic process as turubulence, a statistical approach is taken. In this section a brief description of the main statistical tools used throughout the thesis will be provided.

2.3.1 The probability density function

Considering a turbulent flow, the velocity field $\overline{U}(x,t)$ is assumed to be random; The *Probability Density Function* (PDF) of such a variable U is a function that describe the relative likelihood for a random variable to assume a certain value. If we know the PDF of a random variable, then all statistical moments of any order are known. To better understand the meaning of a PDF we need to introduce another concept which is the *Cumulative Distribution Function* (CDF) which is defined by the following relation:

$$F_u(h) \equiv P(\overline{U}(x,t) \leq h). \tag{2.14}$$

In other words,"$F_u(h)$ is the probability that our random variable $U(x,t)$ assumes a value which is smaller ore equal to h. Every CDF posses the following three properties: $F_u(-\infty) = 0$, $F_u(+\infty) = 1$ and is a monotone non-decreasing function. The probability density function $f(U)$ is now definded as:

$$f(U) \equiv \frac{dF(U)}{dU}, \tag{2.15}$$

and posses the following properties

$$f(U) \geq 0, \tag{2.16}$$

$$\int_{-\infty}^{+\infty} f(U)dU = 1. \tag{2.17}$$

2.3.2 Statistical moments

The *mean* of U is the first order statistical moment and is defined as:

$$\langle \overline{U} \rangle \equiv \int_{-\infty}^{+\infty} \overline{U} f(\overline{U}) dU. \tag{2.18}$$

From the mean, the *fluctuation* is defined as follow:

$$u \equiv \overline{U} - \langle \overline{U} \rangle, \tag{2.19}$$

due to the fact that the mean of a fluctuation is always null, higher moments needs to be introduced. The second order moment is known as *Variance*:

$$\langle u^2 \rangle = \int_{-\infty}^{+\infty} u^2 f(u) dU, \tag{2.20}$$

the square root of the variance is the *Standard Deviation* or *root mean square* (rms); typically gives a measure to the fluctuations' magnitude and is denoted as:

$$\sigma_u = \sqrt{\langle u^2 \rangle}. \tag{2.21}$$

Likewise, other statistical moments can be introduced, i.e. in general the $n-th$ moment

$$\langle u^n \rangle = \int_{-\infty}^{+\infty} u^n f(u) dU, \tag{2.22}$$

Of particular interest in turbulence studies, are the third and fourth order moments, the *Skewness* and *Flatness*; usually they are normalized with the rms of the reference order, giving the skewness and flatness factors:

$$S_u = \frac{\langle u^3 \rangle}{\sigma_u^3}, \tag{2.23}$$

$$F_u = \frac{\langle u^4 \rangle}{\sigma_u^4}. \tag{2.24}$$

Skewness and flatness factors are used to describe some properties of the PDF: the skewness is a measure of the symmetry of the PDF, so is equal to

zero when a PDF is symmetrical, the flatness on the other hand indicates the relative peakedness of the distribution function. Considering a Gaussian Distribution, $S_u = 0$ and $F_u = 3$.

2.3.3 Averages

In turbulence studies, velocity or other quantities are usually divided into their mean value and fluctuating part, thorough the so-called *Reynolds Decomposition*

$$U_i = \langle U_i \rangle + u_i, \tag{2.25}$$

where U_i represents the ith component of the instantaneous velocity vector $U(x,t)$, $\langle U_i \rangle$ is its mean part and u_i its fluctuations. The rigorous way to obtain the averaged value would be the *ensemble average*. Considering than a *Statistically stable* flow, in other words, their statistical properties are not time dependent, we will obtain:

$$\langle U_i \rangle(\mathbf{x}) = \overline{U_i}(\mathbf{x}) = \int_0^T U_i(\mathbf{x}, t) dt. \tag{2.26}$$

Where $\mathbf{x}$ represents the measuring point at time t. If we now consider simulations of homogeneous turbulence, spatial average can be performed. taking a cubic domain of side $\mathcal{L}$, spatial average of $\overline{U}(x,t)$ is defined by:

$$\langle U_i(t) \rangle_{\mathcal{L}} \equiv \frac{1}{\mathcal{L}^3} \int_0^{\mathcal{L}} \int_0^{\mathcal{L}} \int_0^{\mathcal{L}} U(x,t) dx_1 dx_2 dx_3. \tag{2.27}$$

2.3.4 Correlation

Considering a random variable, U which is completely characterized by its PDF, $f(U)$; if we now take the same velocity, but as a function of time, $U(t)$, we will have a *random process*. Even if the PDF is known in a certain place inside our flow field, this does not help us in understanding if there will be some relation within two different points. For this purpose multi-time and multi-space statistical tools are needed. The *auto-covariance* at the point $\mathbf{x}$

will be:

$$R(\mathbf{x}, \tau) \equiv \langle u(\mathbf{x}, t) u(\mathbf{x}, t + \tau), \tag{2.28}$$

where τ is defined as *lag time*, if the considered process is statistically stationary, then the auto-covariance does not depend on t but only on τ. In this way we could have an idea of the time needed for a flow to "forget" its past history at some precise point. Proceeding, we can define the *correlation function* as follows:

$$\rho(\mathbf{x}, \tau) \equiv \frac{\langle u(\mathbf{x}, t) u(\mathbf{x}, t + \tau) \rangle}{\langle u(\mathbf{x}, t)^2 \rangle}, \tag{2.29}$$

and it has the following properties:

$$\rho(0) = 1, \tag{2.30}$$

$$|\rho(\tau)| \leq 1. \tag{2.31}$$

Usually, for processes arising in turbulent flows, we expect that the correlation will diminish as the lag time τ increases. A time scale called *integral time scale* can be defined:

$$\Lambda_t = \int_0^\infty \rho(\tau) d\tau. \tag{2.32}$$

As we did for time, the same considerations can be performed for space, where *covariance* becomes a multi-space and single time statistical property:

$$R_u = (\mathbf{x}, r) \equiv \langle u(\mathbf{x}, t) u(\mathbf{x} + \mathbf{r}, t). \tag{2.33}$$

Than, the *spatial correlation function* will be:

$$\rho_u(\mathbf{x}, r) \equiv \frac{\langle u(\mathbf{x}, t) u(\mathbf{x} + \mathbf{r}, t) \rangle}{\langle u(\mathbf{x}, t)^2 \rangle}. \tag{2.34}$$

In our case, $\mathbf{r}$ represents the distance vector between $\mathbf{x}$ and the other point where we will collect fluctuations. Just as the temporal case, an *integral*

length scale can be defined:

$$\Lambda_l \equiv \int_0^\infty \rho_u(r)dr. \tag{2.35}$$

2.3.5 Power Spectral Density

As we said, the complete description of a random process can be deduced solely from its PDF. Moreover, correlations give us information about space and time evolution of such processes, the spectra will give us information on how the energy is distributed across different frequencies. In order to compute the spectra, the *Fourier Transform* $\mathcal{F}$ can be used. The Fourier transform, converts a mathematical function of time, $f(t)$ into a new function $\mathcal{F}(\omega)$, where ω represents its argument and is the angular frequency; often, $\mathcal{F}(\omega)$ is known as frequency domain, whereas $f(t)$ represent the time domain of the same event:

$$\mathcal{F}(\omega) \equiv \frac{1}{2\pi} \int_{-\infty}^{+\infty} e^{-i\omega t} f(t)dt. \tag{2.36}$$

In this way, for continuous signals, makes sense the introduction of the *Power Spectral Density* (PSD), which describe how the power of a signal is distributed over different frequencies:

$$P = \lim_{T\to\infty} \frac{1}{T} \int_0^{+\infty} \langle u(t)^2 \rangle dt. \tag{2.37}$$

However, for many signals this Fourier transform does not exist. In such way, could be extremely useful the introduction of the *Truncated Fourier Transform* $\mathcal{F}_T(\omega)$, where the considered signal is integrated over a finite interval:

$$\mathcal{F}_T(\omega) = \frac{1}{\sqrt{T}} \int_0^T u(t)e^{-i\omega t}dt. \tag{2.38}$$

The power spectral density will then be:

$$S_{uu}(\omega) = \lim_{T\to\infty} \langle \mathcal{F}_T(\omega)^2 \rangle. \tag{2.39}$$

Of great importance, if we are considering a statistically steady process, our PSD will consitutes a Fourier transform paired with the auto-covariance function $R(\tau)$:

$$S_{uu} = \frac{1}{2\pi} \int_{-\infty}^{+\infty} e^{-i\omega\tau} R(\tau) d\tau. \tag{2.40}$$

where the inverse transform is represented by:

$$R(\tau) = \int_{-\infty}^{+\infty} e^{i\omega\tau} S_{uu}(\omega) d\omega, \tag{2.41}$$

considering that $\tau = 0$ we will end up with:

$$\overline{u^2} = \int_{-\infty}^{+\infty} S_{uu}(\omega) d\omega. \tag{2.42}$$

$S_{uu}(\omega)$ can be interpreted as the turbulence intensity present in the band $d\omega$ centered around ω.

2.4 Channel flow and Turbulence scaling

Most common turbulent flows are bounded by one or more solid surfaces; we can split bounded flows mainly into two diffent groups :

- *Internal Flows*
  - Pipe flow
  - Channel flow
- *External Flows*
  - Flow around ships' hulls and aircraft
  - Atmospheric boundary layer
  - flow of rivers

During the present work we have concentrated our efforts on studying differnt aspects of a channel flow. While in free shear flows turbulence is mainly

caused by differences in flow field, in our case, wall bounded one, turbulence arises due to the presence of a wall, which due to the viscosity of the fluid and to the no-slip condition causes this phenomena.

2.4.1 Description of the flow

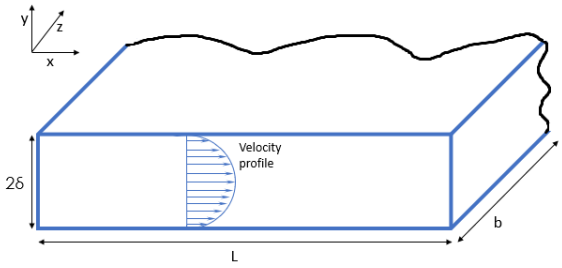

Figure 2.1: Sketch of channel flow

As we can see in Fig. 2.1, we consider a flow through a duct of heigh $h = 2\delta$, length $L/\delta \gg 1$ and aspect ratio $b/\delta \gg 1$. The mean flow is predominantly in the streamwise direction (x), with a variation of the velocity mainly in wall-normal direction (y); the bottom and the top of the channel are at $y = -\delta$ and $y = \delta$, respectively, with the mean plane located at $y = 0$. Moreover the extent of the channel in spanwise direction is large compared to δ thus the flow is statistically independent of z. In order to characterize the flow, we introduce two principal Reynolds numbers:

$$Re_b = \frac{2\delta\overline{U}}{\nu}, \tag{2.43}$$

$$Re_{cl} = \frac{\delta U_{cl}}{\nu}, \tag{2.44}$$

where Re_b and Re_{cl} are,respectively, the Reynolds number obtained from bulk velocity and centreline velocity. Following the classical analysis, wall bounded turbulent flows can be divided into two regions: an *inner region*

close to the wall, and an *outer region* far away from it. Furthermore, inside the inner region, flow viscosity plays a major role, while in the outer region it does not. Inside the inner region, the variables that affect most the mean velocity $\overline{U}$ are: the wall friction τ_w, the wall-normal distance y and the fluid kinematic viscosity ν. Since skin friction for channel flow is defined as follows:

$$\tau = \mu \frac{d\overline{U}}{dy} - \rho \overline{uv}, \tag{2.45}$$

and the wall friction is:

$$\tau_w \equiv \tau(-\delta), \tag{2.46}$$

Moreover one could demonstrate that τ has a linear relation with respect to τ_w as follows:

$$\tau = \tau_w \left(1 - \frac{y}{\delta}\right), \tag{2.47}$$

which represent a linear relationship, decreasing from wall where $\tau = \tau_w$ to the centerline where $\tau = 0$. Therefore we can introduce an appropriate velocity and length scale inside the near-wall region, starting from the *friction velocity*

$$u_\tau = \sqrt{\frac{\tau_w}{\rho}}, \tag{2.48}$$

and a *viscous lengthscale*

$$\delta_\nu = \frac{\nu}{u_\tau}. \tag{2.49}$$

A characteristics Reynolds number based on viscous scales, known as *friction Reynolds number* is defined by:

$$Re_\tau = \frac{u_\tau \delta}{\nu} = \frac{\delta}{\delta_\nu}. \tag{2.50}$$

Also, we can normalize the distance from the wall in viscous lengths or *wall units* denoted as:

$$y^+ = \frac{y}{\delta_\nu} = \frac{y u_\tau}{\nu}. \tag{2.51}$$

There are different regions or layers, in the near-wall region, defined on the basis of relations (2.44); The *viscous wall region*, $y^+ < 50$ is where we have a direct effect of molecular viscosity on the shear stress; the *outer region*,

$y^+ > 50$ the direct effect of viscosity is negligible, moreover, within the wall region, inside the *viscous sublayer* $y^+ < 5$, Reynolds shear stresses are negligible if compared to viscosity. Furthermore, it is important to mention that if we increase the Reynolds number, the dimension of the layer will decrease. As we obtained y^+ normalizing the distance from the wall, we can perform the same manipulation for the velocity:

$$u^+ = \frac{\langle U \rangle}{u_\tau}, \tag{2.52}$$

which, after some manipulation will look like:

$$u^+ = f(y^+). \tag{2.53}$$

Which is known as *Prandtl's law of the wall* (1926); for a more in-depth background the reader is directed to Pope [13] .

Temperature is treated in a slightly different way, the reference temperature is set to 1, thus in order to compute viscous temperature we need to divide not dimensional temperature T^* with friction temperature T_τ as follows:

$$T^+ = \frac{T^*}{T_\tau}. \tag{2.54}$$

Where:

$$T_\tau = \frac{\dot{q}|_w}{u_\tau} = \frac{1}{Re_\tau Pr} \left.\frac{dT}{dy}\right|_w \tag{2.55}$$

2.4.2 Energy cascade

As mentioned above, one of the main characteristics of a turbulent flow is the presence of a wide range of different scales/eddies. One can observe the macroscopic features associated to geometry of the flow, which in our case will be represented by the half-height, δ, of the channel. The idea of an energy cascade was first introduced by Richardson, stating that turbulent kinetic energy is first introduced at large scales through a production mechanism, then transferred via inviscid way to smaller scales until it dissipates into heat at small scales through viscous forces. According to Richardson, eddies

can be characterized by length l, velocity $u(l)$ and time scale $\tau(l)$; at big scales, eddies have dimensions l_0 , comparable with channel dimensions; a characteristics velocity u_0 which is within the order of magnitude of the rms of the turbulent intensity. After some years, Kolmogorov (1941) theorized the smaller dissipative scales, known so far by his name; he formulated a theory that could be summarized in three hypothesis:

1. At sufficiently high Reynolds number, small scales turbulence is statistically isotropic.

2. At sufficiently high Reynolds number, statistics at small scales, $l \ll l_0$ have universal form determined by ν and ϵ which is the mean dissipation rate of energy.

This is mainly caused by the fact that at small scales dissipation of energy transferred from bigger scales happens through viscous process; we can define length, velocity and time scales of the dissipation range:

$$\eta \equiv \left(\frac{\nu^3}{\epsilon}\right)^{1/4}, \tag{2.56}$$

$$u_\eta \equiv (\epsilon\nu)^{1/4}, \tag{2.57}$$

$$\tau_\eta \equiv \left(\frac{\nu}{\epsilon}\right)^{1/2}, \tag{2.58}$$

where η is the Kolmogorov length scale. Also he derived the ratio between large and dissipative eddies sizes:

$$\frac{l_0}{\eta} \approx Re^{3/4}, \tag{2.59}$$

stating that if we increase the Reynolds number, the range of scales between l_0 and η will increase as well. In other words, it expresses the concept of *scale separation* in high Reynolds number flows. As the Reynolds number increases the difference between η and l_0 increases nearly linearly.

3. At sufficiently high Reynolds number, statistics for scales l, with $\eta \ll l \ll l_0$ have a universal form determined solely by ϵ and independent of ν.

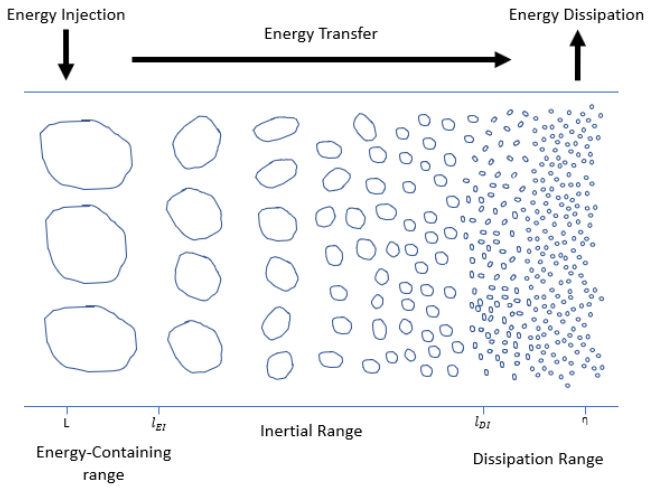

Figure 2.2: Energy cascade scheme

The new range introduced in the third theory is the so-called *inertial subrange* it is only marginally affected by viscosity, depends almost exclusively on energy transfer rate. In Fig. 2.2 we show a scheme of the energy cascade process.

Chapter 3

Hot Wire Anemometry

Hot-wire anemometry (HWA) remains, by far, one of the most used techniques for velocity measurements in the field of turbulent research. Its first introduction by King (1914) gives outstanding performances in terms of spatial and temporal resolutions at a fraction of the cost of optical measurements techniques. In Fig. 3.1 a sketch of a single wire sensor is depicted. The main disadvantage is represented by the intrusive nature of the measurements and the fact that a simple single wire sensor is limited to a point measurement of one velocity component. Hot wire measurements are based on a simple

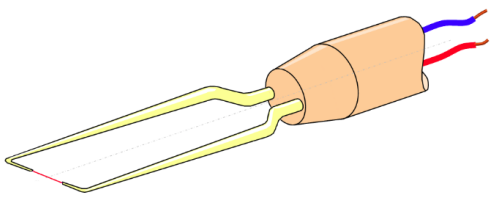

Figure 3.1: Single wire sensor

principle: the heated wire will experience some cooling effect by the flow. Mainly, this effect is caused by forced convection heat losses, which have strong velocity dependency. In case this heat is measurable, e.g. through a temperature dependent resistance of the sensor, than, using calibration techniques, we can retrieve velocity from cooling rate of the wire. Nowadays

hot-wire anemometry works in constant temperature mode (CTA), meaning that the temperature of the wire is kept constant by continuously changing the current intensity at the tip of the wire. For more in-sight we suggest the reader to check Örlü [12] and Compte-Bellot [3].

3.1 Basic principles

As already mentioned, the principle of thermal anemometer is that the amount of cooling experienced by a heated wire, whose electrical resistance depends on temperature, can be related to the local flow velocity. Hence, HWA is based on a thermoelectric measurements principle. Let us assume that the hot wire is electrically heated through a current I, than, the heating power from Joule heating will be:

$$P = IE = I^2 R_w = \frac{E^2}{R_w}, \tag{3.1}$$

where E denotes the voltage drop across the hot-wire sensor and R_w is the resistance of the heated wire; since the cooling is mainly caused by forced convection W:

$$W = hA_w(T_w - T_0) = h\pi DL(T_w - T_0), \tag{3.2}$$

where h is the convective heat transfer coefficient, D is the wire diameter, L is own length, T_w and T_0 indicates respectively the temperature of the wire and its surrounding medium; usually for our applications this $\Delta T = T_w - T_0$ is around 200 $^\circ K$. For a metal, R_w can be expressed as a function of T_w, using a linear approximation around a certain reference temperature T_0:

$$R_w = R_0[1 + \alpha_0(T_w - T_0)], \tag{3.3}$$

where R_0 and α_0 are respectively the wire resistance at T_0 and the resistivity coefficient of the wire material. If we consider metals, this value is positive, meaning that for an increase in resistance we will face a temperature increase.

Considering the fluid at ambient temperature, it is possible to derive the following expression:

$$T_w - T_a = \frac{R_w - R_a}{\alpha_a R_a}. \tag{3.4}$$

a refers to ambient condition; if we consider a cylinder-shaped body, the forced convection coefficient h can be expressed as follows:

$$h = \frac{Nuk_f}{D}, \tag{3.5}$$

where k_f represents the thermal conductivity of the fluid, Nu is the Nusselt number, that, neglecting free convection and for a low subsonic flow will be function of:

$$Nu = f(Re, Pr). \tag{3.6}$$

Introducing now a_T which represents the over-heat ratio, one of the main contribution during the operative life of an hot wire:

$$a_T = \frac{T_w - T_0}{T_0}. \tag{3.7}$$

Furthermore we can express the Nusselt number with a correlation function in the following form:

$$Nu = A_1 + B_1 Re^n, \tag{3.8}$$

$$Nu = A_2 + B_2 U^n, \tag{3.9}$$

where A, B and n are characteristics constant parameter of the considered correlation function. Combining the correlation function with W we will first obtain:

$$\frac{I_w^2 R_w}{R_w - R_a} = A + BU^n. \tag{3.10}$$

Considering the voltage drop E across the hot-wire, eq. (3.10) becomes:

$$\frac{E_w^2}{R_w} = (A + BU^n)(T_w - T_a). \tag{3.11}$$

Term α_0 was included in the constant A and B; if we consider the CTA operation mode, $(T_w - T_a)$ and R_w are constants and can be incorporated in A and B:

$$E^2 = A + BU^n. \tag{3.12}$$

which is the so-called King's law, where A, B and n can be obtained from calibration tecniques.

3.2 Spatial resolution

As mentioned above, despite the very good spatial resolution of hot wire sensors, at high Reynolds number, turbulent structures have dimensions of Kolmogorov scales η, however, HWA have finite length that is larger than η and responds to an averaged value of the turbulent fluctuations $u(t)$; the measured velocity fluctuations will read:

$$u_m(t) = \left(\frac{1}{L} \int_{-L/2}^{L/2} u(s,t) ds \right)^{1/n}. \tag{3.13}$$

The subscript m refers to the measured quantity, L is the wire length and n denotes the non-linear relation between heat exchange and velocity. The main effect on the measured quantities results in an attenuation of the measured velocity variance. This effect is well known since the first era of the hot-wire. Dryden [4] in 1937 studied the effects of a not complete homogeneity of velocity fluctuations across the wire on measurements of velocity correlation, connected to scale of turbulence. However, for wall turbulence, the isotropy hypothesis is not guaranteed near the wall, where high velocity gradient are expected, thus, higher effect of spatial averaging are achieved in the near wall region. The spatial resolution effect starts then to be investigated intensively since the eighties, using wire of different length, like Johansson and Alfredsson did in 1983 [6]. After many years of research, a rule of thumb has been introduced, $L^+ < 20$ so that HWA will not be significantly affected by spatial resolution problems, while length to diameter ratio should be $L/D > 200$ to avoid end conduction effect. Several correction

schemes are developed in order to compensate spatial averaging error, one could check Segalini et al. [15].

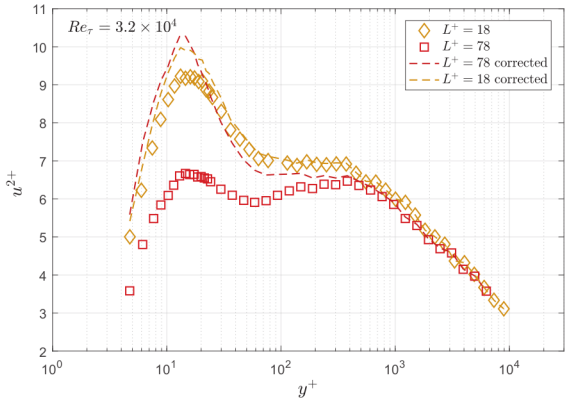

Figure 3.2: Inner scaled streamwise variance for $Re_\tau \approx 3.2 \cdot 10^4$, Plot taken from Fiorini PhD Thesis [1]

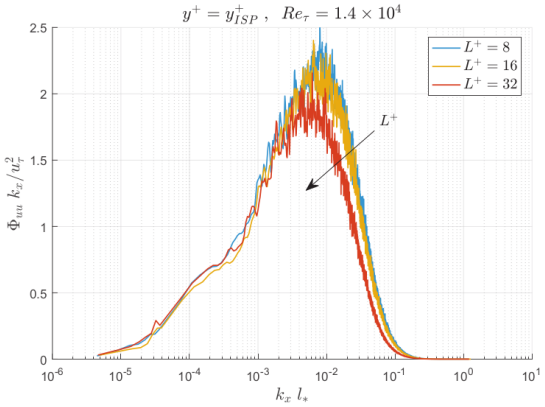

Figure 3.3: Pre-multiplied inner-normalized power spectral density at the location $y^+ = y^+_{ISP}$ (inner spectral peak) for $Re_\tau = 1.4 \cdot 10^4$ and different sensor lengths, Plot taken from Fiorini PhD Thesis [1]

As Fig. 3.2 and 3.3 shows, we can see the effect of spatial averaging caused by the characteristics dimension of the sensing element. Increasing the dimension of the anemometer will result in a decrease of the fluctuations captured by the HWA due to their characteristic dimension, which are smaller than the sensor itself.

3.3 Temperature correction

Wind tunnel experiments are performed at different ambient temperature, also, the fan inside a facility could heat the flow increasing the temperature. In order to obtain comparable results among experiments, velocity should be corrected for different temperature values. Let us start from eq (3.11):

$$\frac{E_w^2}{R_w} = (A + BU^n)(T_w - T_a) = f(U)(T_w - T_a), \tag{3.14}$$

would become:

$$E_w^2(T_{ref}) = f(U)(T_w - T_{ref}). \tag{3.15}$$

Where the subscript $_{ref}$ stands for the laboratory reference temperature, used during calibration procedure. $E_w(T_{ref})$ represents the voltage drop that hot-wire measures when is surrounded by a fluid at T_{ref}. We consider temperature as a passive scalar, thus it not influences flow dynamics, velocity dependence for both eq. (3.14) and (3.15) is supposed to be equal:

$$\frac{E_w^2(T_a)}{E_w^2(T_{ref})} = \frac{T_w - T_a}{T_w - T_{ref}}, \tag{3.16}$$

$$E_w^2(T_{ref}) = E_w^2(T_a)\left(\frac{T_w - T_a}{T_w - T_{ref}}\right)^{-1}. \tag{3.17}$$

Plugging the over heat ration a_T from eq. (3.7) will allow us to re-shape eq. (3.17) as follows:

$$E_w^2(T_{ref}) = E_w^2(T_a)\left(1 - \frac{T_a - T_{ref}}{\alpha_T/\alpha_{el}}\right)^{-1}. \tag{3.18}$$

Only two experimental parameter as α_T and α_{el} are presents, among them, only the electrical resistivity is unknown, since the over heat ratio is fixed by the user.

3.4 CCA and CTA

Hot wire sensors mainly are divided in two operational modes: constant current mode or constant temperature mode

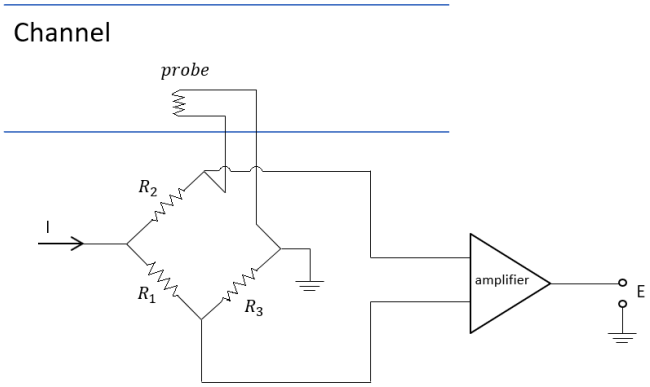

Figure 3.4: Constant Current Anemometry scheme

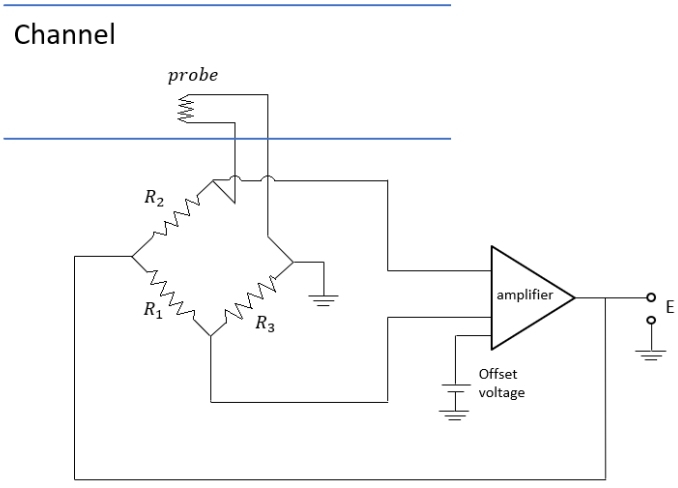

Figure 3.5: Constant Temperature Anemometer scheme

In both cases, the wire is placed inside a Wheatstone bridge. As one can see from the Figures above, hot wire is represented by one of the four

resistance. If we consider CCA, as Fig 3.4, current across the wire is kept constant, thus flow fluctuations cause temperature variation on the wire, hence its resistance. These fluctuations causes variations on the voltage measured at the tip of the bridge:

$$E = IR(T). \tag{3.19}$$

This bridge voltage is then related to one of the wire and to the velocity field. Their introduction was mainly caused by a lack technology when stabilizing the temperature on CTA. As one can see in Fig.3.5 constant temperature anemometer are based on a control feedback, where temperature of the wire is supposed to be kept constant. This system is inherently unstable, thus feedback loop is needed to keep the temperature constant. Nowadays they are widely used. In order to keep constant the resistance, heat produced by the wire should change accordingly to flow fluctuations.

Chapter 4

Spectral Method

Inside this chapter we will give a brief description on the numerical scheme and codes used to perform our simulations; The entire mathematical formulation would result heavy, for simplicity we focused our attention to spatial and temporal discretization.

4.1 Simson

A pseudo-**S**pectral Solver for **I**nco**M**pre**S**sible B**O**u**N**dary Layer Flows, also known as **SIMSON**, is a code entirely developed at Kunglinga Tekniska Högskolan (KTH), by Mattias Chevalier, Philipp Schlatter, Anders Lundhbladh and Dan S. Henningson. It implements spectral integration technique to solve Navier-Stokes for incompressible channel or Boundary layer flows. Originally written in Fortran 77/90, can be used as a solver for Direct Numerical Simulation (DNS) or Large Eddy Simulation (LES). Different passive scalars can be computed. The code can be run in serial and throughout parallelization, thanks to Message Passing Interface (MPI). In order to solve the problem, wall parallel directions are discretized using Fourier expansion, wall-normal directions using Chebyshev series and Time is discretized using a third order Runge-Kutta scheme and Cranck-Nicolson method.[2]

4.2 Temporal discretization

The time advancement is carried out by two different scheme, let us consider the equation:

$$\frac{\partial \psi}{\partial t} = G + L\psi. \tag{4.1}$$

where ψ could represent our vorticity terms or the passive scalar; G contains the non-linear terms and L represents the linear diffusion. Operator L is discretized using a second order accurate Crank-Nicolson and G is discretized explicitly by a third order, three or four stage Runge-Kutta (RK3 or 4) scheme. In such way, eq. (2.36) may be written as follows

$$\psi^{n+1} = \psi^n + a_n G^n + b_n G^{n-1} + (a_n + b_n)\left(\frac{L\psi^{n+1} + L\psi^n}{2}\right). \tag{4.2}$$

where a_n and b_n are chosen according to the explicit scheme used, G and L are assumed to have an explicit time dependency. Since the scheme has three or four stages, a full phisical time step is only achieved every three or four iterations. We can apply the time advancement scheme to equation (2.9) and (2.10) obtaining:

$$\begin{aligned}\left(1 - \frac{a_n + b_m}{2Re}\nabla^2\right)\psi^{n+1} = \left(1 + \frac{a_n + b_n}{2Re}\nabla^2\right)\psi^n + a_n h_v + b_n h_v^{n-1}, \\ \nabla^2 v^{n+1} = \psi^{n+1}.\end{aligned} \tag{4.3}$$

and

$$\left(1 - \frac{a_n + b_n}{2Re}\nabla^2\right)\omega^{n+1} = \left(1 + \frac{a_n + b_n}{2Re}\nabla^2\right)\omega^n + a_n h_\omega + b_n h_\omega^{n-1}. \tag{4.4}$$

4.3 Horizontal discretization - Fourier expansion

The discretization in the horizontal directions, in our case represented by x and z, uses a Fourier series expansion which assumes a periodic solution. Streamwise and spanwise dependence of each variable could be written as

follows:

$$u(x,z) = \sum_{l=-\left(\frac{N_x}{2}-1\right)}^{\frac{N_x}{2}-1} \sum_{m=-\left(\frac{N_z}{2}-1\right)}^{\frac{N_z}{2}-1} \hat{u}(\alpha_l, \beta_m) e^{i(\alpha_l x + \beta_m z)}. \tag{4.5}$$

where $\alpha_l = 2\pi l/x_L$, $\beta_m = 2\pi m/z_L$; N_x and N_z represents the number of Fourier modes included in the respective directions; α and β represents the wavenumber. We can now expand eq. (2.42) and (2.43) in Fourier series obtaining three equations as follows:

$$\begin{aligned} (D^2 - \lambda^2)\hat{\psi}^{n+1} &= \hat{f_v}^n, \\ (D^2 - k^2)\hat{v}^{n+1} &= \hat{\psi}^{n+1}, \\ (D^2 - \lambda^2)\hat{\omega}^{n+1} &= \hat{f_\omega}^n. \end{aligned} \tag{4.6}$$

where

$$\begin{aligned} \lambda^2 &= k^2 + \frac{2Re}{a_n + b_n}, \\ \hat{f_v}^n &= \hat{p_v}^n + \frac{2Re}{a_n + b_n}\hat{h_v}^n, \\ \hat{f_\omega}^n &= \hat{p_\omega}^n + \frac{2Rea_n}{a_n + b_n}\hat{h_\omega}^n. \end{aligned} \tag{4.7}$$

$\hat{p_v}^n$, $\hat{p_\omega}^n$ are terms that collect the respective partial right hand side of the euqations. Once found $\hat{v}$ and $\hat{\omega}$ we can proceed and solve equation (1.2) and the equation of normal vorticity, both transformed to Fourier space. we will then find u and w.

4.4 Normal discretization - Chebyshev expansion

So far, we have derived second order constant coefficient ordinary differential equation of the form:

$$\begin{aligned}(D^2-\kappa)\hat{\chi} &= \hat{f},\\ \hat{\chi}(0) &= \gamma_{-1},\\ \hat{\chi}(y_L) &= \gamma_1.\end{aligned} \tag{4.8}$$

once mapped the interval $[0, y_l]$ to $[-1, 1]$, we can solve accurately the equation expanding in Chebyshev series: χ, it's second derivative, f and the boundary conditions:

$$\hat{\chi}(y) = \sum_{j=0}^{N_y} \tilde{\chi}_j T_j(y), \tag{4.9a}$$

$$D^2\hat{\chi}(y) = \sum_{j=0}^{N_y} \tilde{\chi}_j^{(2)} T_j(y), \tag{4.9b}$$

$$\hat{f}(y) = \sum_{j=0}^{N_y} \tilde{f}_j T_j(y), \tag{4.9c}$$

$$\hat{\chi}(1) = \sum_{j=0}^{N_y} \tilde{\chi}_j = \gamma_1, \tag{4.9d}$$

$$\hat{\chi}(-1) = \sum_{j=0}^{N_y} (-1)^j \tilde{\chi}_j = \gamma_{-1}, \tag{4.9e}$$

$$D\hat{\chi}(1) = \sum_{j=0}^{N_y} j^2 \tilde{\chi}_j = \delta_1, \tag{4.9f}$$

$$D\hat{\chi}(-1) = \sum_{j=0}^{N_y} j^2 (-1)^{j+1} \tilde{\chi}_j = \delta_{-1}. \tag{4.9g}$$

T_j represents the Chebyshev polynomial of order j and N_y is the highest order of polynomial included in the expansion. Combining expansions with

eq.4.8 we will find the following relation between the coefficients:

$$\tilde{\chi}_j^{(2)} - \kappa\tilde{\chi}_j = \tilde{f}_j, \qquad j = 0, ..., N_y. \tag{4.10}$$

Finally we can find the relations of $\hat{\chi}$ with respect ro its derivative, which we can use for integration or differentiation:

$$\tilde{\chi}_j^{(p)} = \sum_{m=j+1}^{N_y} m\tilde{\chi}_m^{(p-1)}, \qquad j = 1, ..., N_y, \tag{4.11a}$$

$$\tilde{\chi}_j^{(p-1)} = \frac{1}{2j}(c_{j-1}\tilde{\chi}_{j-1}^{(p)} - \tilde{\chi}_{j+1}^{(p)}) \qquad j = 1, ..., N_y. \tag{4.11b}$$

p indicates the order of the derivative and $c_j = 2$ for $j = 0$ and $c_j = 0$ for $j > 0$. Looking at the first differentiation relation one can observe that an error in the highest order coefficient of $\tilde{\chi}^{(p-1)}$ influences all coefficients of its derivatives $\tilde{\chi}^p$. This problem could be overcome by the usage of the Chebishev integration method (CIM) even thogh a truncation error is introduced.

4.5 Domain, Initial and Boundary condition

In order to perform simulations on Simson we will need to set up different informations regarding the computational domain as well as boundary and initial conditions.

4.5.1 Computational domain

Since Simson is a pseudo spectral method, our domain will be defined by number of spectral modes assigned to a physical domain defined in different scripts. The parameters file **par.f** contains all information regarding a simulation and need to be adjusted before every compilation of the code. The parameter **nx**, **ny-1** and **nz** represents the spectral modes in each directions of the domain. They must be even and factorable by at least 2. Also, inside the aforementioned script one need to specify the number of cores needed for the parallelization of the code. Remembering that cores and spectral modes

need to be one multiple with each other, not to cause a segmentation error when compiling. The physical domain, is then defined inside **bls.i** script, here we need to specify the dimensions of our domain normalized with respect to half channel height h.

4.5.2 Initial conditions

The information regarding initial conditions are handled by two script: **bls.i** and **fsc.i**; in the first we define the type of flow we intend to run, any disturbances as well as the Reynolds number, usually normalized with respect the center line velocity. The second script contains information regarding similarity solutions for boundary layers flows; here we will specify, convergence criterion, wall normal resolution and scalar that need to be solved. Of particular interest is the fact that here we will need to specify the Pr, Prandtl number and general boundary condition, i.e. we need to define if one will use an isothermal or an iso-flux boundary condition.

4.5.3 Boundary conditions

Once specified Domain and initial condition; boundary condition need to be fixed both for the flow and scalar quantity we intend to solve. **bla.i** and **fsc.i** will be helpful scripts in this phases of the set up. Inside the first script, all basic informations related to the simulations are specified, starting from times, file needed to be compiled and fields that will be saved throughout the run. **bla.i** is sequential and will contains a voice named **ibc** that will contain a number specifying the boundary condition for the flow. proceeding inside the same script we will find **tbc**, there, one need to specify the boundary condition set for the scalar which will be solved.

Chapter 5

Methodology and Validation procedure

Inside this chapter we will show the reader the entire validation process carried out during the thesis, starting from a channel flow, as reported in Fig. 5.1 . After considering the Forcing terms as stand alone cases, we will end with the implementation of the Constant current anemometer.

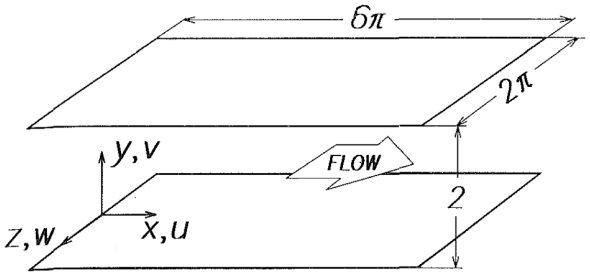

Figure 5.1: Sketch of the geometry of the channel flow domain; where x,y and z are respectively the streamwise, wall-normal and spanwise direction

5.1 Simulation characteristics

The Validation process started considering a turbulent channel flow of the following specifications:

Axis	**Dimensions**	**Modes**	**grid spacing**
x	4π	128	$17.67\,\Delta x^+$
y	2	129	$0.055\,\Delta y^+$
z	2π	128	$8.84\,\Delta z^+$

Following the test case inside Simson, the Reynolds number, based on half width of the channel and the centre line velocity is equal to 4200 which corresponds to a Re_τ approximately equal to 180. Also we could parallelize our simulations up to 64 cores, half of the modes over z. Since the computational burden of such simulation would result quite heavy, as a debug test, we decrease the number of modes by a factor 2; in this way we are able to obtain results qualitatively right, without waiting too much time. As we mentioned in the spectral element method chapter, y direction is discretized with Chebishev polynomial, thus corresponding to a spacing smaller near the wall.

5.2 Channel Flow Statistics

As every simulations ended, we export the statistics using a fortran script inside simson, in order to plot every information using the preferred software, in our case we take advantage of the reliability of Matlab.

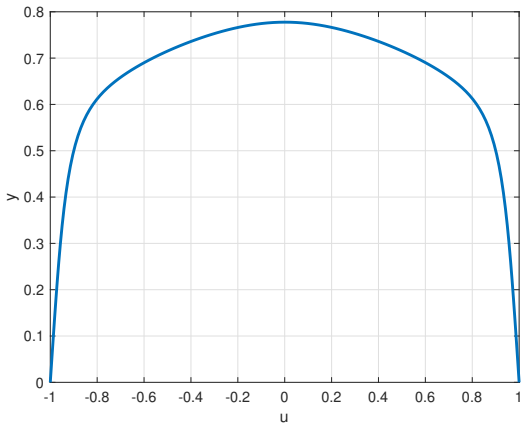

Figure 5.2: Velocity profile,u, scaled with global quantity

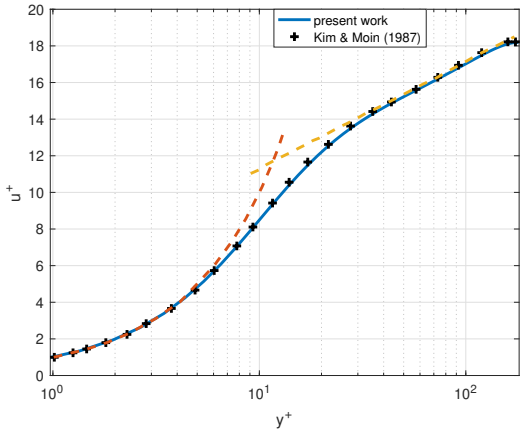

Figure 5.3: Blue solid line represent the present work, '+' black symbols represents data from Kim & Moin paper, yellow dashed line represent the 'Log law' $u^+ = 2.5lny^+ + 5.5$, orange dashed line represent the law of the wall $u^+ = y^+$

Fig. 5.2 and 5.3 shows the stream wise component of the velocity, i.e. u scaled with the local free stream and the displacement thickness for the outer scale and wall units for the inner scale plot.

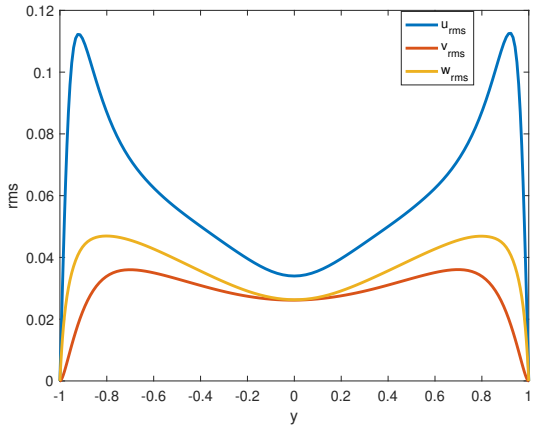

Figure 5.4: Velocity rms, outer scaled, blu line represents the streamwise component, orange line represents the span wise component and red line represent the wall-normal component of the velocity

Fig. 5.4 and 5.5 depicts the rms profiles respectively outer scaled and in wall units; the inner scaled plot is also compared with results obtained by Kim & Moin in 1987 [9]. It's clear from plot that results shows a good behaviour even though the mesh is coarser with respect to the one used on the paper. The peak of turbulence intensity, regarding the u component is located at $y^+ = 15$, thus confirming the goodness of the obtained results.

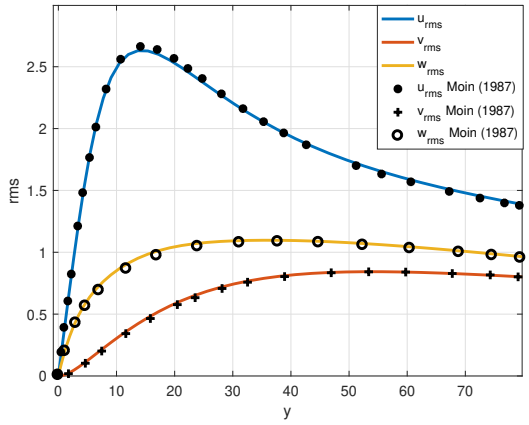

Figure 5.5: Velocity rms, inner scaled, blu line represents the streamwise component, orange line represents the span wise component and red line represent the wall-normal component of the velocity; dot, circle and plus are data taken from Kim & Moin results

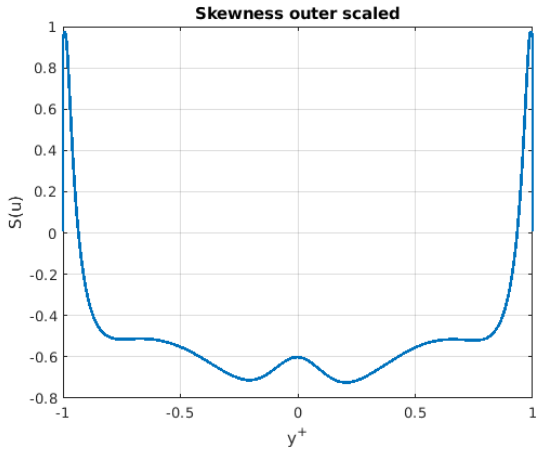

Figure 5.6: Skewness, $S(u)$

We also reports in Fig. 5.6 and 5.7 respectively the skewness and flatness for the streamwise component of the velocity, scaled with global quantity.

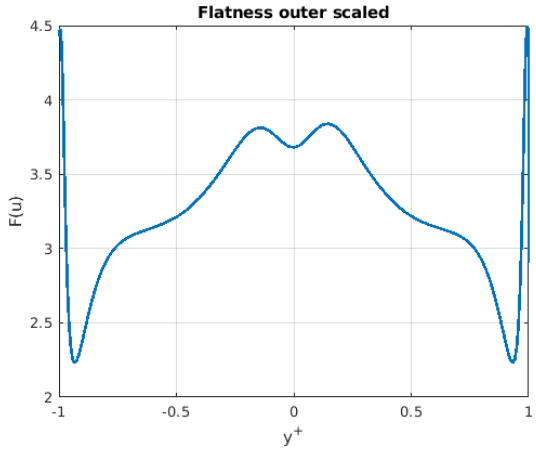

Figure 5.7: Flatness, $F(u)$

5.3 Volume Forcing

The introduction of the forcing term was performed following the paper proposed by Kasagi et al. on 1992 [7] which presented a DNS of passive scalar field in a turbulent channel flow. While the Boundary conditions for the velocity are defined simply by the no-slip condition and hence their implementation is performed setting the velocity equal to zero at the wall as a Dirichlet condition; regarding thermal boundary condition the modelling becomes more complex. There are different possibilities when one has to deal with heat balance and in this field, boundary conditions could become really complex and hard to implement. Usually there are two main conditions: Isothermal case, where a value of the temperature is fixed; and Iso-flux case, where derivative of the temperature are fixed.

5.3.1 Implementation and Boundary condition

First it has to be decided if one wants to have constant temperature, meaning Dirichlet, or constant heat flux, Neumann condition at the wall boundary. In the latter case, constant heat flux through the wall is fixed, meaning that one can add or subtract heat per unit wall accordingly to the heat injected in the channel. In our case, as did by Kasagi in 1997,

we implemented isothermal boundary conditions: as we can see in Fig. 5.8

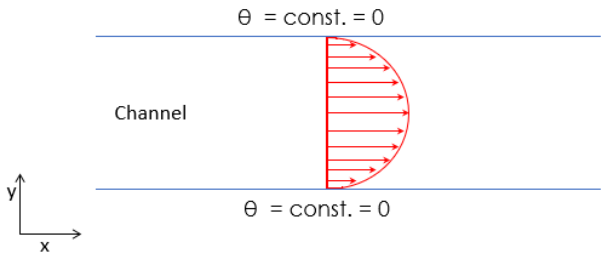

Figure 5.8: Isotherm boundary condtion sketch

Temperature is fixed at both wall boundary, thus is constant over time and channel length. The governing equation for the thermal field is given as follows:

$$\frac{\partial \theta}{\partial t} = -u_i \frac{\partial \theta}{\partial x_i} + \frac{1}{RePr} \nabla^2 \theta + u\theta \tag{5.1}$$

where Pr is the Prandtl number and the last term of the right hand side represent the forcing term. As the fluctuations of the temperature are assumed to be zero, the boundary condition, for isothermal condition are given:

$$\theta(x, 0, z, t) = \theta(x, 2, z, t) = 0 \tag{5.2}$$

furthermore the initial thermal field will be:

$$\theta(x, y, z, 0) = Pr \cdot u(x, y, z, 0) \tag{5.3}$$

5.3.2 Statistics

To be sure that the flow was fully developed, 5000 time steps were waited before collecting statistics and than, 10000 more time steps were performed. The results obtained are then compared with the one obtained by Kasagi et al.(1992)[7] and the one by Kim and Moin (1989 and 1987)[9] [8].

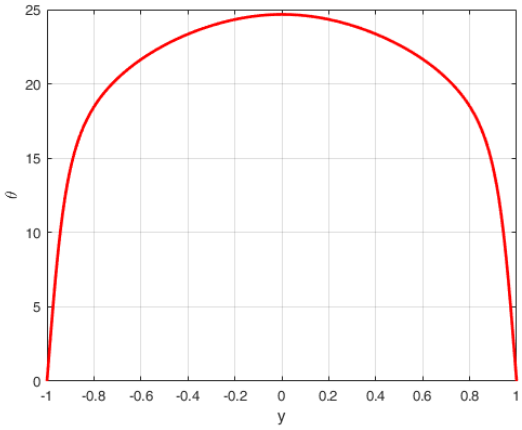

Figure 5.9: Temperature Profile, outer scaled

in Fig. 5.9 we show the temperature profile outer scaled, while on Fig. 5.10 we compared the temperature and velocity profile with ones obtained by Kasagi and Kim & Moin. Both profiles, clearly match the results obtained in both papers.

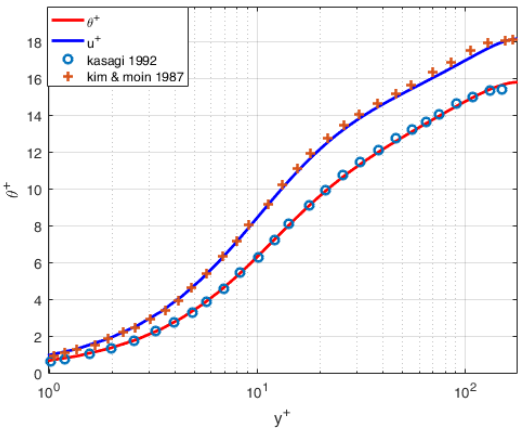

Figure 5.10: red solid line represent the temperature profile, blu solid line represent the velocity profile, + are results from Kim & Moin, circle are results from Kasagi inner scaled

In Fig. 5.11 and 5.12 we have plotted temperature root mean square, outer scaled alone and inner scaled coupled with u_{rms} and the results obtained by Kasagi. Also in *rms* plot the matching is clear, as expected.

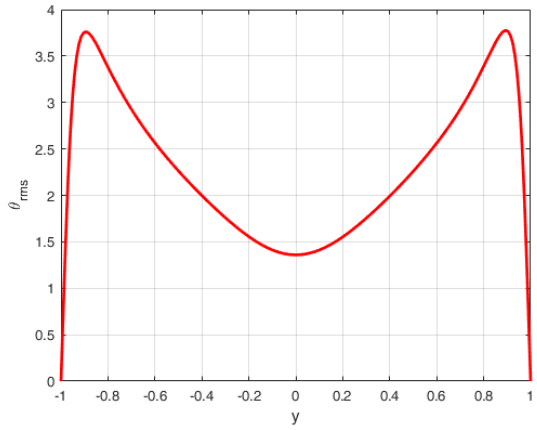

Figure 5.11: Temperature rms, outer scaled

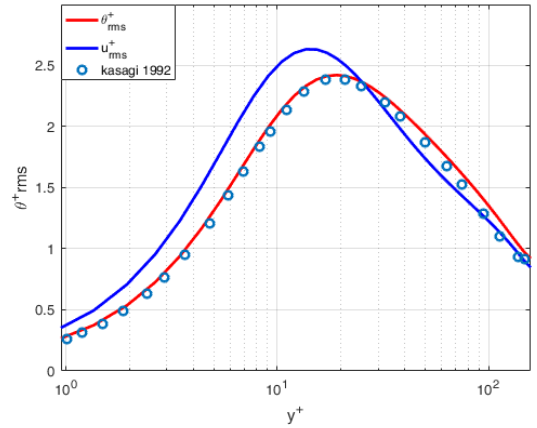

Figure 5.12: Blue solid line represent the rms of the streamwise component of the velocity, red solid line represents the temperature rms and blue circles are results obtained by Kasagi

Now we will show to the reader plot regarding $u\theta$ and $v\theta$ both alone and compared with Kasagi results.

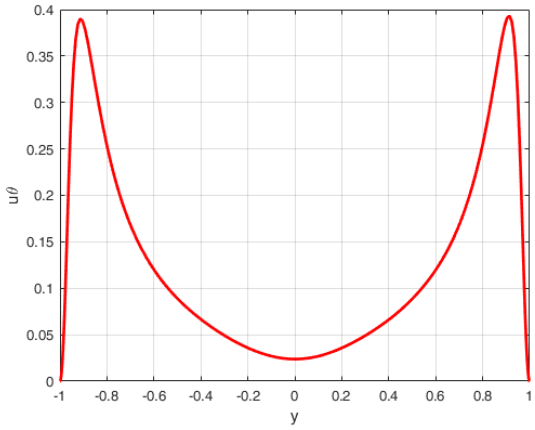

Figure 5.13: $u\theta$, outer scaled

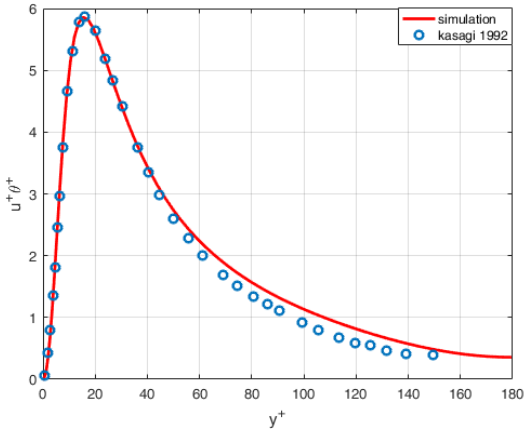

Figure 5.14: red solid line represents the $u^+\theta^+$, inner scaled, dots are data from Kasagi.

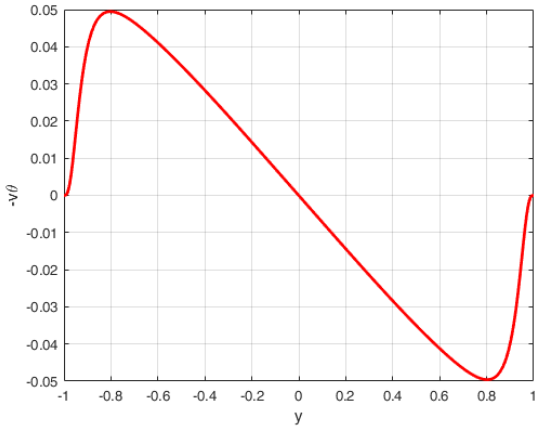

Figure 5.15: $-v\theta$, outer scaled

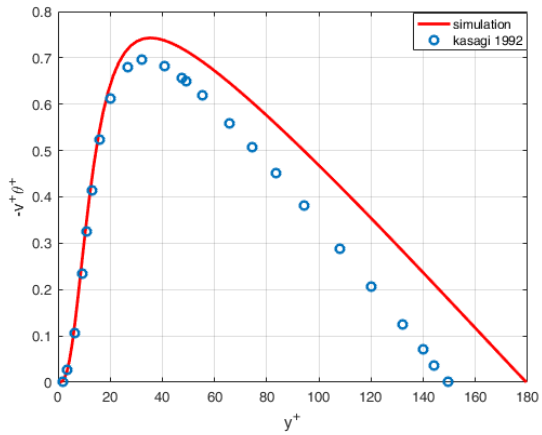

Figure 5.16: $-v\theta$, inner scaled, dots are results from Kasagi

Finally, Skewness and Flatness for the temperature are reported here:

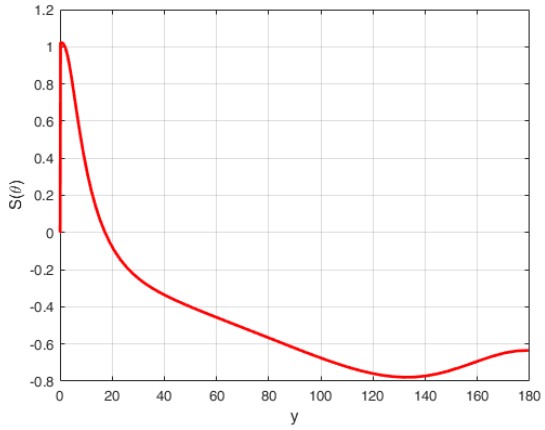

Figure 5.17: $S(\theta)$, skewness for the temperature

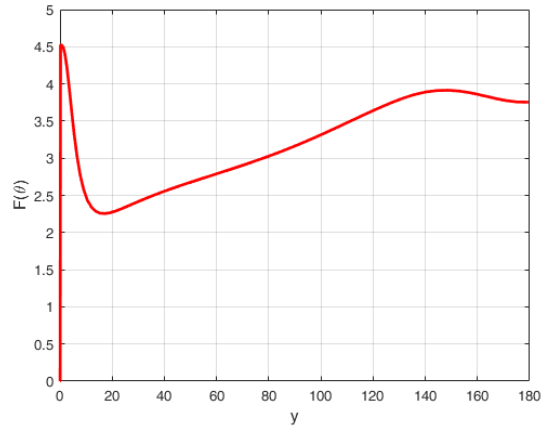

Figure 5.18: $F(\theta)$, flatness for the temperature

As one can see from the plot showed in the previous pages, all quantities, like scalar profile, rms, skewness and flatness presents a trend that follow quite precisely the considered papers by Kasagi and by Kim & Moin. We decide to implement the volume heating at a temperature near the ambient one, as could be in experimental condition, where T tends to be imposed as constant as possible and not too far from the ambient of the considered facility.

5.4 Line Source

Plugging the forcing term represented by the volume heating was the second step on the validation process performed during the thesis The natural proceeding, since an hot-wire is represented by a small line of heat immersed on a flow field, would be the implementation of a line source of heat. On Simson, we do not have the possibility to implement complex geometry as could be a real hot-wire. This is due to the nature of the code. We implemented a line source in the channel as a forcing term, represented by two Gaussian distribution, one across the streamwise (x) and the other along wall-normal (y):

$$f(x) = e^{\left(\frac{x-x_o}{x_s}\right)^2}, \tag{5.4}$$

$$f(y) = e^{\left(\frac{y-y_o}{y_s}\right)^2}. \tag{5.5}$$

where the subscript $_o$ and $_s$ are respectively the position in the channel and the scale.

$$\frac{\partial \theta}{\partial t} = -u_i \frac{\partial \theta}{\partial x_i} + \frac{1}{RePr}\nabla^2\theta + L_{x-y} \tag{5.6}$$

Where L_{x-y} represents the combination of the Gaussian:

$$L_{x-y} = A \cdot f(x) \cdot f(y) = A \cdot e^{\left(\frac{x-x_o}{x_s}\right)^2} \cdot e^{\left(\frac{y-y_o}{y_s}\right)^2} \tag{5.7}$$

A represents the overall amplitude of the two Gaussian distributions. In this way we can play with the overall amplitude of the Gaussian, changing A magnitude and with x and y scales, changing the magnitude of x_s and y_s:

In Fig. 5.19 is shown how the line is placed inside the channel; the two combined Gaussian distribution allow us to place in a precise position over x and y our source of heat, while it cross the channel over the span-wise direction.

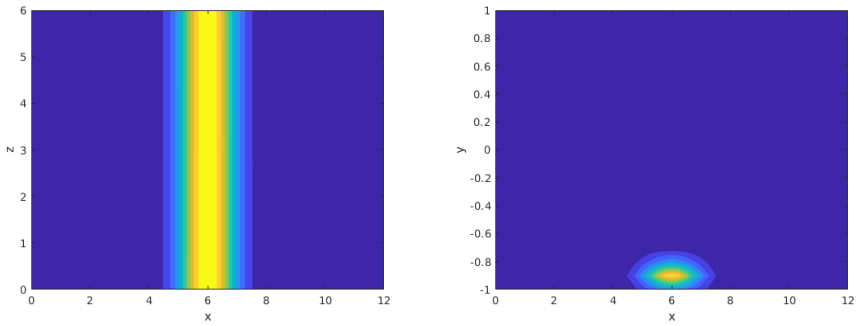

Figure 5.19: Line Source implementation in a Contour plot, xz plane on left, xy plane on right; contour level from 0 (blue) to 1 (yellow)

5.4.1 Statistics

In order to verify the presence of the line we run different simulations at various heat amplitude; Checking each time temperature and velocity field. Here we will show temperature profile at line source position and rms distribution.

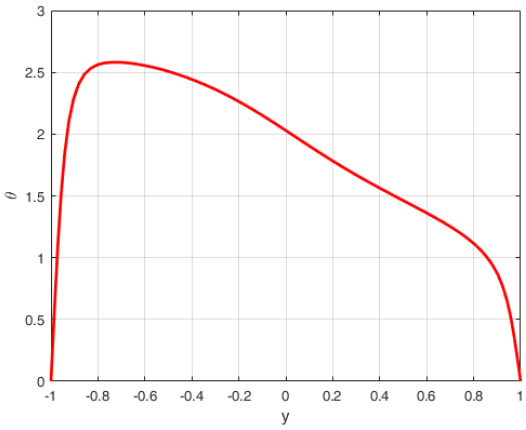

Figure 5.20: Temperature Profile at line source position

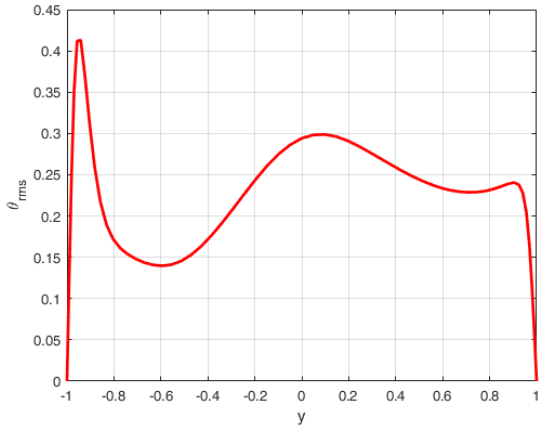

Figure 5.21: Temperature root mean square at line source position

as one can see both on Fig. 5.20 and 5.21 the presence of the line cause a non-symmetric behaviour if compared to the previous cases.

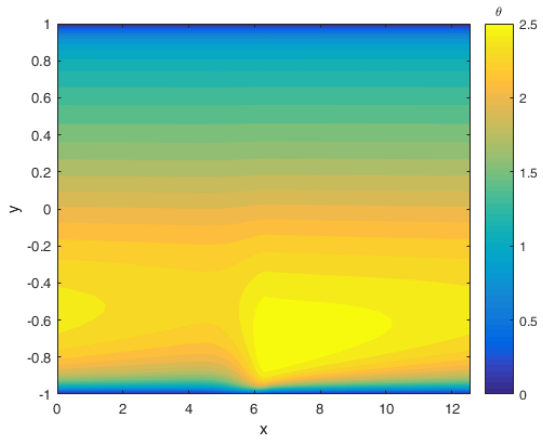

Figure 5.22: Iso-contours of the passive scalar values in the xy plane, Contour levels from 0(blue) to 2.5 (yellow)

In Fig. 5.22 we plotted a plane x, y of the channel to let the reader clearly see the presence of the line. Adding the line source inside the code as a combined exponential over x and y allow us to effectively validate the presence of a heat source, as one can see in Fig. 5.20 the profile present a non symmetric behaviour since the line is the unique source of heat inside our channel. Moreover, the rms profile, plotted in Fig.5.21 confirm this fact. At

the end, to confirm that the channel was effectively heating up, even though the scalar intensity was not that high we performed a contour plot of $x - y$ "slice" of our test case. Clearly we can see the position of the line at $x = 2\pi$ and $y = -0.9$.

5.5 Constant Current Anemometer

The last step of the validation process was the combination of the two forcing term: the volume heating and the line source. In this way we are able to mimic the behaviour of a Constant Current anemometer.

5.5.1 Definition of the problem

Constant Current anemometer, as depicted in Fig. 3.4 are designed so that the current across the wire kept constant. A change in temperature and resistance occur, the resultance change in voltage is the calibrated against the velocity. Following this idea, we implement both Volume heating and line source of heat at the same time.

$$\frac{\partial \theta}{\partial t} = -u_i \frac{\partial \theta}{\partial x_i} + \frac{1}{RePr} \nabla^2 \theta + u\theta + L_{x-y} \tag{5.8}$$

Where u_i Since the turbulence intensity, as expected found is maximum value at $y^+ = 15$ we are interested in placing there our line source in order to see how it will affect the flow field.

Forcing	**Details**	
Line source	Amplitude	1
	Position	$x = 2\pi\,, y = -0.9$
	x,y scales	$x = 1\,, y = 1$
Volume heating	Amplitude	1

as we can see, simulation details about the forcing terms are reported in the table above, we started from 64 spectral modes to access qualitatively the goodness of the results before moving to higher spectral modes, which will negatively affect to the computational burden.

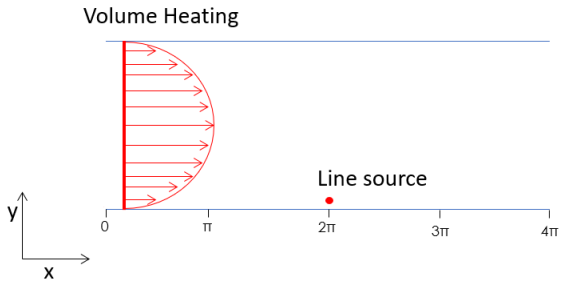

Figure 5.23: sketch of the channel with line source and volume heating implemented

We checked the full developed flow condition after 2500 ν/u_τ^2, as we can see from Fig.5.24 we plotted statistics collected until the 2600 ν/u_τ^2 compared to few time-steps statistics collected after the considered simulation time. As one can see from the figure, we used rms quantity of the velocity to validate the fully developed condition.

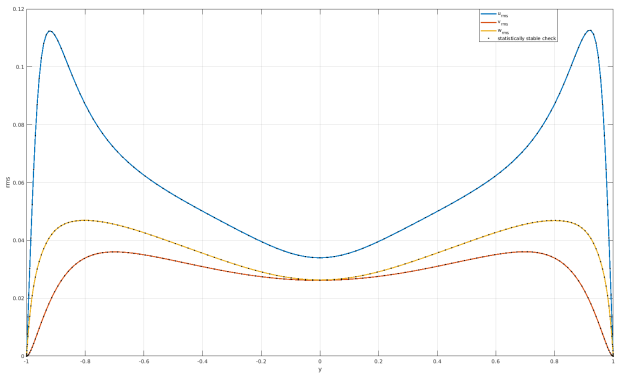

Figure 5.24: Velocity rms, outer scaled, blu line represents the streamwise component, orange line represents the span wise component and red line represent the wall-normal component of the velocity, dots are full developed condition check

Once checked that our flow was statistically stable we continue the simulation for about 15000 time-steps before ending the simulation.

5.5.2 Preliminary results

Here we will show the results obtained following the presented characteristics, starting from temperature profile, rms and other quantities.

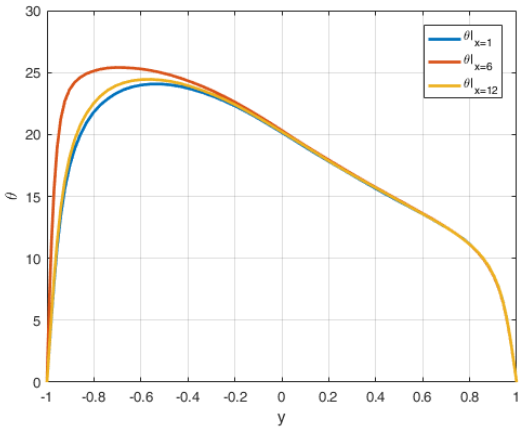

Figure 5.25: Temperature Profile scaled with global quantity, blue solid line represent θ profile at $x = 1$,red solid line represent θ profile at $x = 6$, line source position and yellow solid line represent θ profile at $x = 12$

As we can see from Fig. 5.25 the presence of the line source influences all the channel, thus our case is not representing what usually happens when an hot-wire is placed inside a duct to measure velocity fluctuations. Moreover, *rms* profiles confirm that our assumption were wrong.

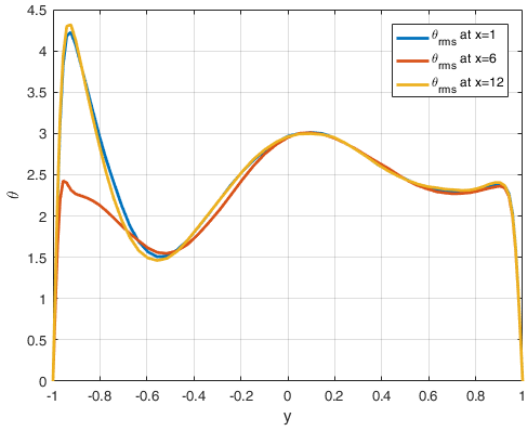

Figure 5.26: Temperature rms scaled with global quantity, blue solid line represent θ_{rms} profile at $x = 1$,red solid line represent θ_{rms} profile at $x = 6$, line source position and yellow solid line represent θ_{rms} profile at $x = 12$

It is clear that the influence of the heat source, placed at half of the channel, is too high, then we also checked the velocity field saved throughout the simulation using visualization software, as one can see in Fig. 5.27:

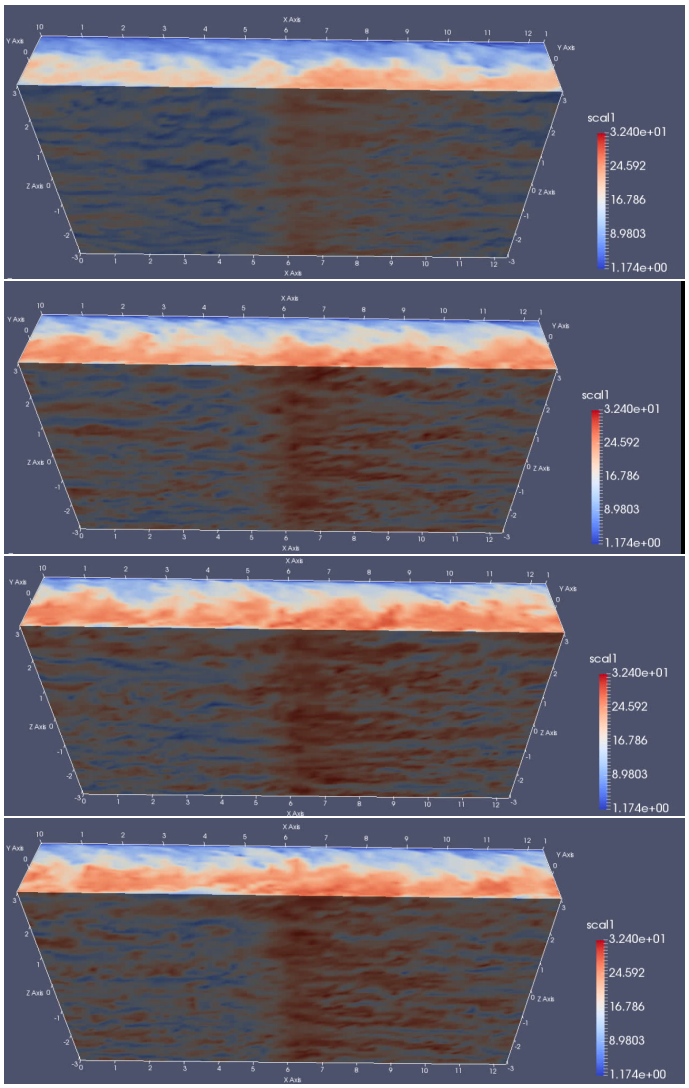

Figure 5.27: snapshots of the temperature behaviour inside the channel, going from $t = 500$ on top, to $t = 10000$ on bottom

Analysing these 4 picture has pointed out that our line source was too large, also the channel dimension are not enough. As one can see from the picture, we are kind of simulating many hot wire on their own wake, this phenomenon is caused by the periodic boundary condition. The flow do not have time to normalize its behaviour after the line source, thus, it re-enter the channel and pass by the line again.

5.5.3 Influence of the channel length

The results obtained from the previous simulation pointed out that channel dimension and line source influences were too large. Following this way of thinking we enlarge our domain and re-shaped the forcing term related to the line source. We decide to enlarge the channel in streamwise direction by a factor of 4, thus reaching $x = 16\pi$ keeping spanwise and wall normal dimension as the previous case. Furthermore we changed slightly the values regarding the line source forcing term:

Forcing	**Details**	
Line source	Amplitude	100
	Position	$x = 8\pi\,, y = -0.9$
	x,y scales	$x = 0.1\,, y = 0.1$

In this way we are able to simulate the channel flow with volume heating and line source as forcing term. Also, enlarging the streamwise direction allow the temperature to normalize again after the line source, so that, when passing from the outlet to the inlet do not cause the effect of having many hot-wire one in the wake of the other.

Chapter 6

Results

Inside this chapter we will report the results obtained from the simulations carried out during the thesis work. Starting from statistics related to velocity we will pass to temperature behaviour and influences caused by the line source presence.

6.1 Simulation details

Once overcome validations procedures we set up the simulation combining all forcing terms considered. The entire validation procedure showed all problems faced during the development of the numerical model. Here we will report information regarding the last simulation performed and used to extract statistics. As we saw that the channel length was not enough to see the "natural behaviour" of an hot-wire sensor, thus we moved to 16π. Moreover, we decided to increase the amplitude of the forcing terms related to x and y dimension of the line; in this way we are able to "reduce" the wire dimensions, getting closer to a real hot-wire. Reducing the dimensions of the line, caused at a first glance a temporary disappearing of the line, so we decided to compensate these effects increasing the overall amplitude of the forcing term related to the line.

Axis	Dimensions	Modes
x	16π	128
y	2	129
z	2π	128

Here we reported the details about channel dimensions and modes used for each of them. Below we show details about the forcing terms used and their relative amplitude.

Forcing	Details	
Line source	Amplitude	100
	Position	$x = 8\pi$, $y = -0.9$
	x,y scales	$x = 0.1$, $y = 0.1$
Volume heating	Amplitude	0.1

We launched the simulation on our cluster, named "Kebnekaise", imposing a total simulation time equal to 15000; while we waited 5000 simulation times before collecting the statistics, time that we consider needed to the flow to become fully developed.

6.2 Turbulent statistics

We will report here statistics related to turbulent velocity field, starting from velocity profile scaled both with global and wall units:

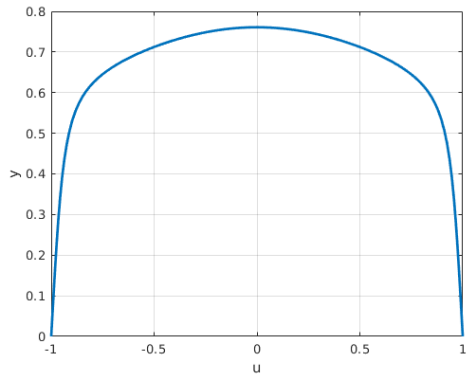

Figure 6.1: Velocity profile, scaled with global quantity

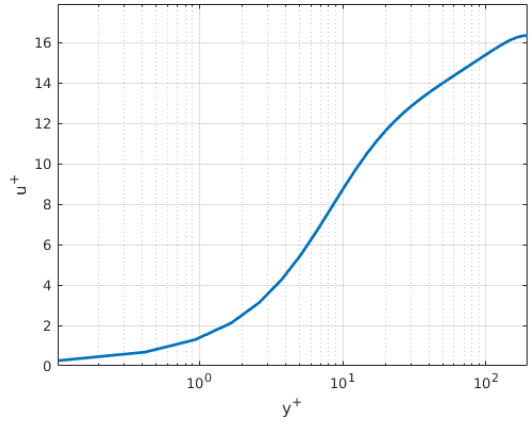

Figure 6.2: Velocity profile, inner scaled

Thus confirming the goodness of the profile if we consider the validation cases. It is clear from the *rms* plot the peak of the turbulence intensity located at $y^+ = 15$.

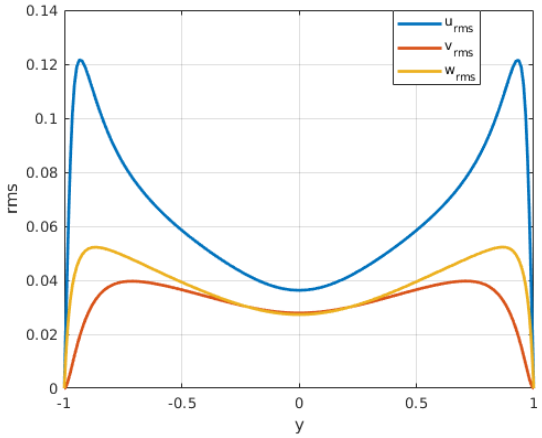

Figure 6.3: Velocity rms, outer scaled, blu line represents the streamwise component, orange line represents the span wise component and red line represent the wall-normal component of the velocity

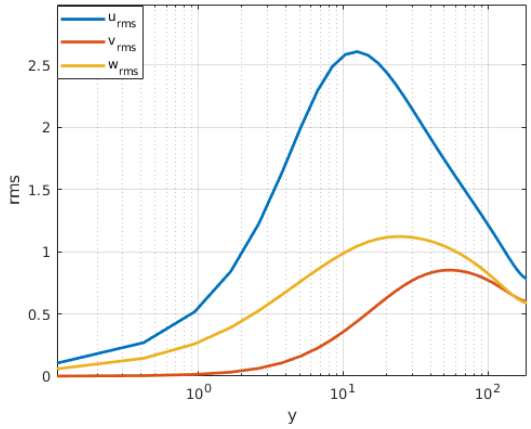

Figure 6.4: Velocity rms, inner scaled, blu line represents the streamwise component, orange line represents the span wise component and red line represent the wall-normal component of the velocity

As done in the previous chapter, we reported here the root mean square behaviour both scaled with global quantity, so half channel height and centre line velocity or scaling wall distance in wall units. Moreover to fully confirm the results obtained so far we compared the skewness and flatness behaviour with the one obtained by Kim & Moin [9]:

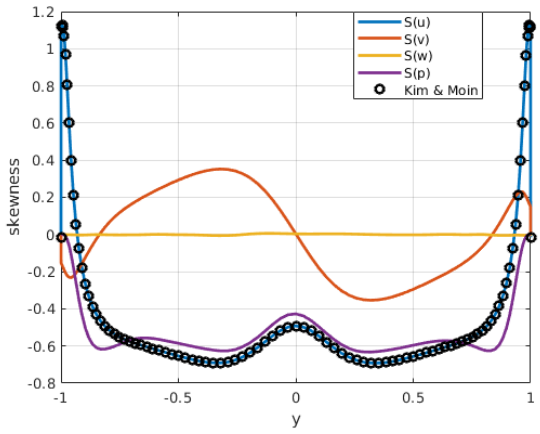

Figure 6.5: Skewness, outer scaled, in blue the stream wise component u, in red wall normal v, in orange the spanwise w, in purple the pressure p and black circles are results obtained by Kim & Moin.

in order to not confuse too much the reader we decide to show only thesSkewness for stream wise component of the velocity, the same has been performed for the flatness plot Results from skewness confirm the behaviour of simulation performed by Kim & Moin [9] even though the w component of the velocity shows some variations, their are confined to small values if compared to stream wise and wall normal component. Also, the pressure shows the correct profile.

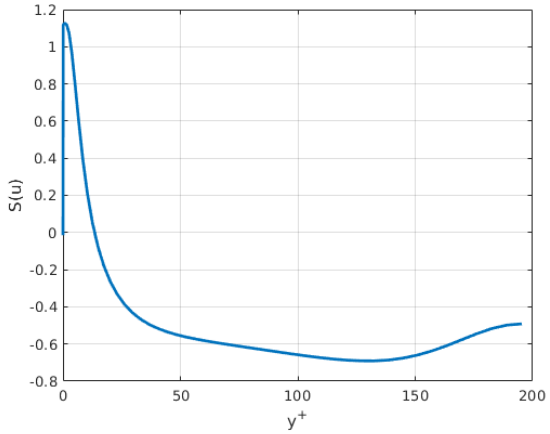

Figure 6.6: Skewness for the stream wise component of the velocity u, inner scaled

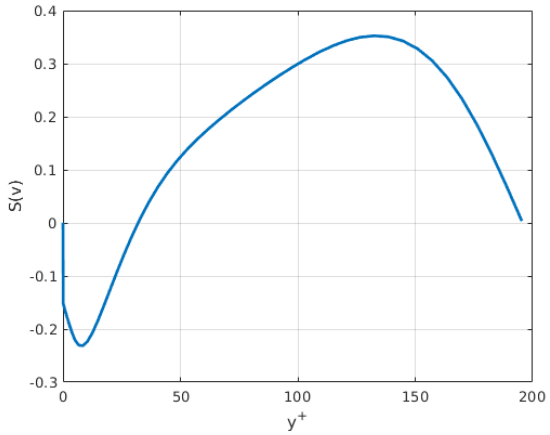

Figure 6.7: Skewness for wall normal component of the velocity v inner scaled

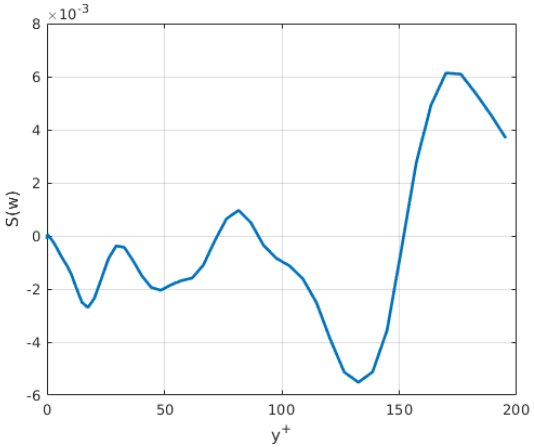

Figure 6.8: Skewness for the span wise component of the velocity w inner scaled

We will show now the flatness, also here, first of all scaled with global quantity, than in wall units. to better understand the plot, also here we divided the inners scaled plot, showing one component at a time to let the reader clearly see the behaviour of the plotted quantity.

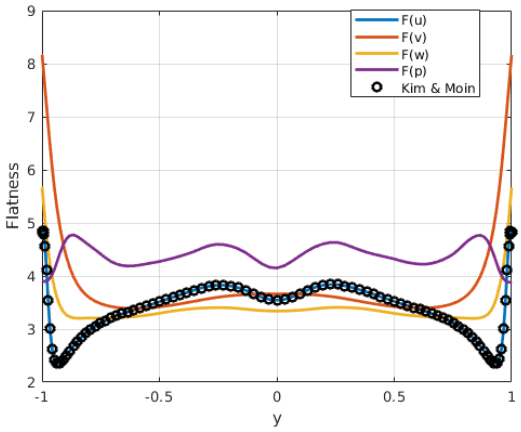

Figure 6.9: Flatness, outer scaled, in blue the stream wise component u, in red wall normal v, in orange the spanwise w , in purple the pressure p and black circles are results obtained by Kim & Moin.

As we did for the skewness, Kim & Moin [9] results confirm the trend of the flatness, both for inner and outer scaled quantity.

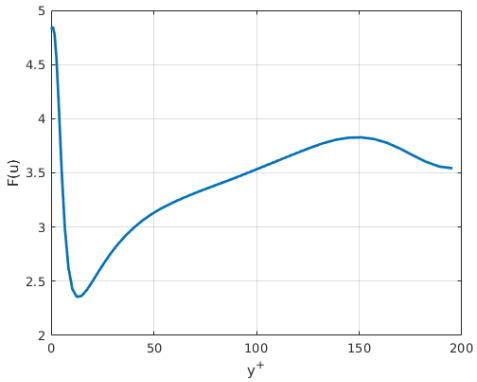

Figure 6.10: Skewness for the stream wise component of the velocity u, inner scaled

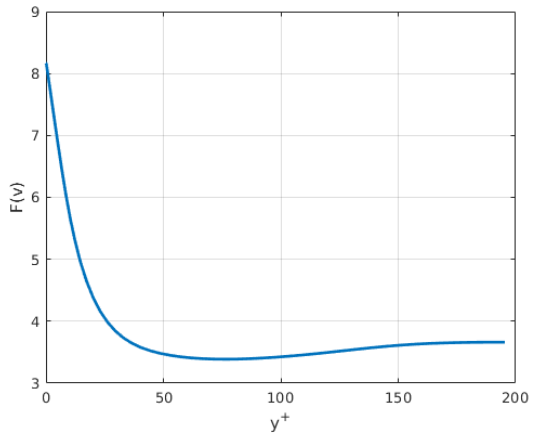

Figure 6.11: Skewness for wall normal component of the velocity v inner scaled

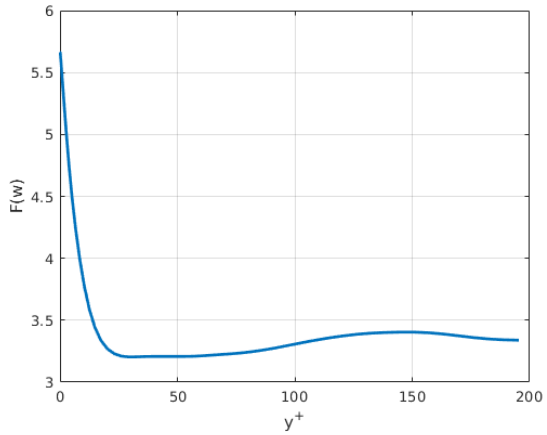

Figure 6.12: Skewness for the span wise component of the velocity w inner scaled

6.3 Temperature statistics

Throughout this section we will show the results regarding temperature statistics; since the isotropy nature of the flow is lost due to the presence of the line source of heat, it is not possible to average the quantity over the stream wise component. The position of the channel will exploit different behaviour accordingly to the presence or not of the line. Moreover, showing quantities before or after the line will also depict different situations.

6.3.1 Statistics at line source position

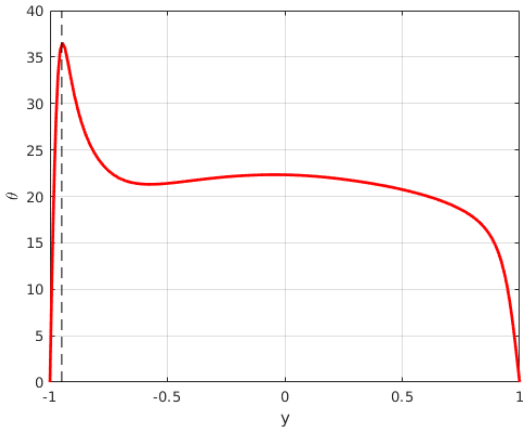

Figure 6.13: θ profile at line source position ($x = 8\pi$), dashed line represents the line source location over y

From fig. 6.13 we can clearly see the presence of the line source, placed at $y^+ \approx 15$. The resultant profile looks non symmetric, presenting a peak at the line position. Of interest could be behaviour of the profile throughout the entire wall normal distance.

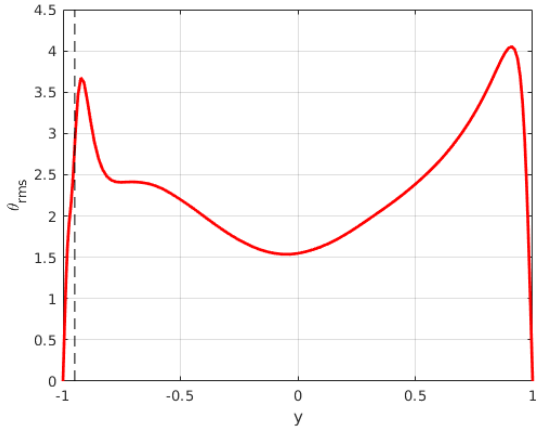

Figure 6.14: θ rms at line source position ($x = 8\pi$) and dashed line represents the line source location over y

Also here, in fig. 6.14 the rms at line source position results in a lower value, in coherence with the physical behaviour. Since the line inject heat in the system continuously, there the fluctuations of the temperature will result lower if compared to the opposite side of the channel.

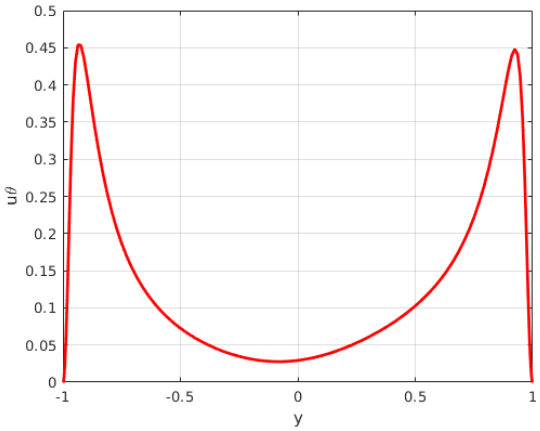

Figure 6.15: $u\theta$ at line source position ($x = 8\pi$)

As one can see from the plot reported below, the symmetry is lost in almost every case, only $u\theta$ seems to keep its symmetric behaviour due to the influence of the velocity field. while other quantity are mainly influenced by the presence of the line.

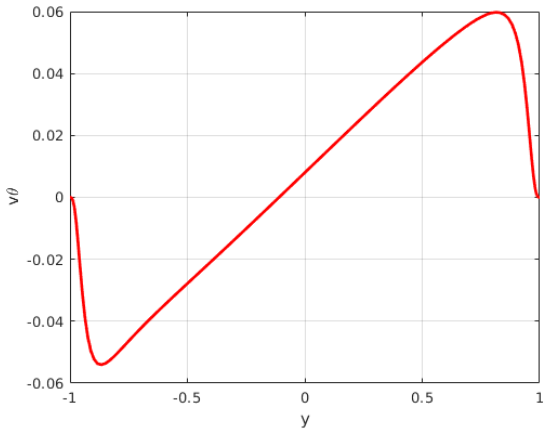

Figure 6.16: $v\theta$ at line source position ($x = 8\pi$)

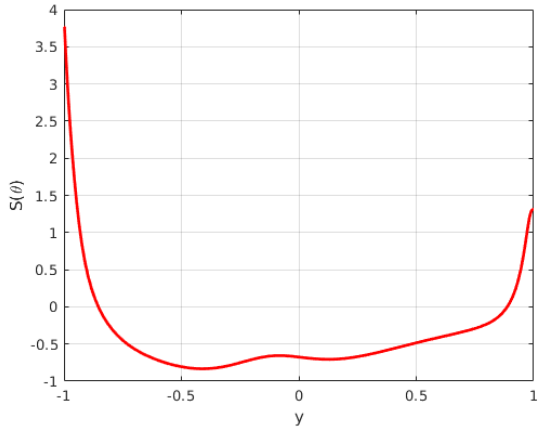

Figure 6.17: $S(\theta)$ at line source position ($x = 8\pi$)

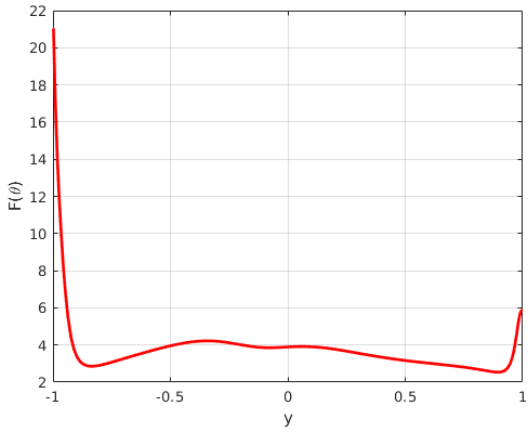

Figure 6.18: $F(\theta)$ at line source position ($x = 8\pi$)

6.3.2 *Statistics at different channel position*

Here we will show statistics at different channel position, pointing our attention to the inlet and the outlet of the channel. As done in the previous section, we will report the plot outer scaled.

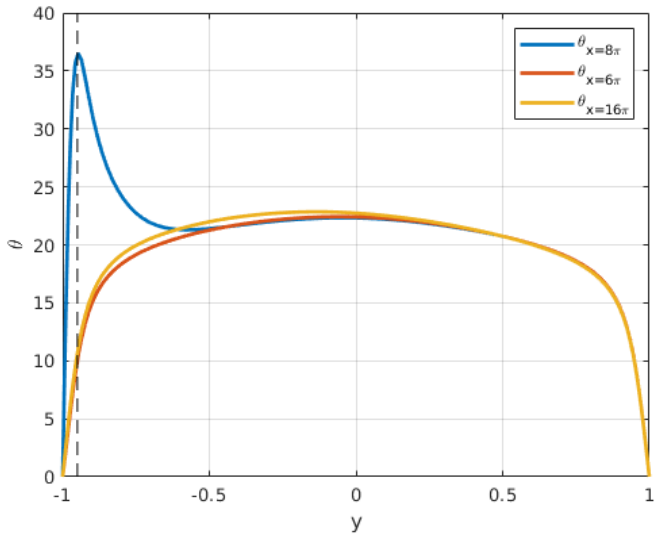

Figure 6.19: θ profile at $x = 6\pi$, $x = 8\pi$ (line source position), $x = 16\pi$ and dashed line represents the line source location over y

Plotting different channel position allow us to understand that the line source influence before, ad after its presence becomes negligible, as should happen in real life, considering that the dimension of the hot wire sensor are negligible if compared to the duct, or the pipe where we will perform our experiments.

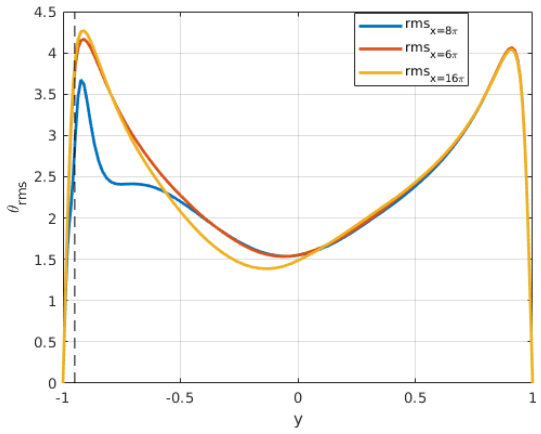

Figure 6.20: θ_{rms} profile at $x = 6\pi$, $x = 8\pi$ (line source position), $x = 16\pi$ and dashed line represents the y location of the line source

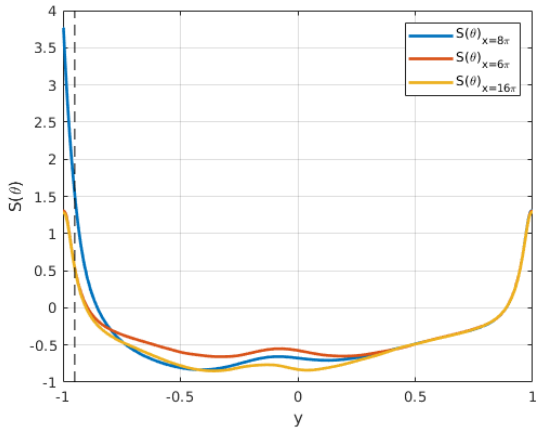

Figure 6.21: $S(\theta)$ profile at $x = 6\pi$, $x = 8\pi$ (line source position), $x = 16\pi$ and dashed line represents the y location of the line source

Also skewness and flatness confirm that the influences of the line source disappear at the outlet of the channel.

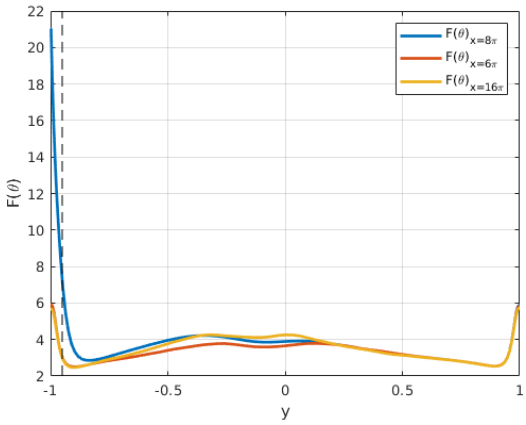

Figure 6.22: $F(\theta)$ profile at $x = 6\pi$, $x = 8\pi$ (line source position), $x = 16\pi$ and dashed line represents the y location of the line source

6.3.3 Statistics after the line source position

Here we will show to the reader the statistics obtained after the line source position, we choose to consider only two positions: $x = 9.5\pi$ and $x = 11\pi$ showing the wake of the heat released by the wire inside the channel.

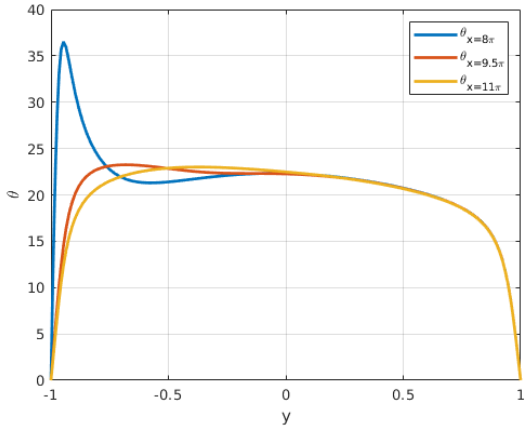

Figure 6.23: θ profile at $x = 8\pi$ (line source position), $x = 9.5\pi$, $x = 11\pi$ and dashed line represents the y location of the line source

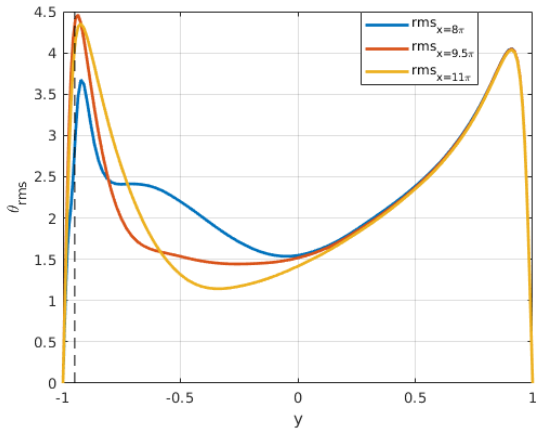

Figure 6.24: θ_{rms} profile at $x = 8\pi$ (line source position), $x = 9.5\pi$, $x = 11\pi$ and dashed line represents the y location of the line source

The plot depicted above shows the temperature falling back to its original position, however from the results we can clearly see that temperature need one third of the overall channel dimension to recover its original shape.

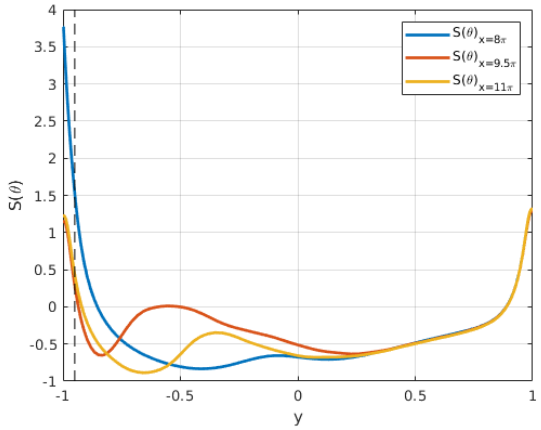

Figure 6.25: $S(\theta)$ profile at $x = 8\pi$ (line source position), $x = 9.5\pi$, $x = 11\pi$ and dashed line represents the y location of the line source

Quantities relates to the passive scalar solved in our simulations shows its behaviour along the entire channel. while its clear that the line did not influence the quantity before the line position, temperature evolution after the line exploit interesting behaviour like lower value of the rms. Of interest

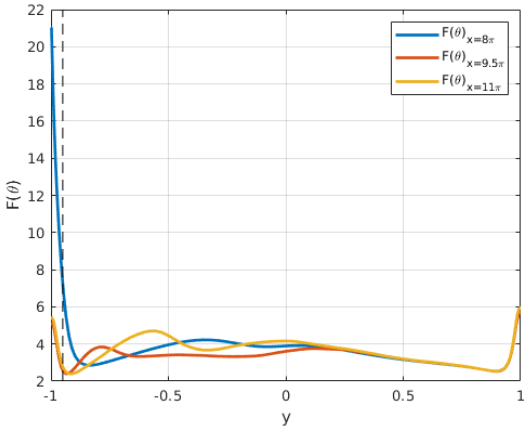

Figure 6.26: $F(\theta)$ profile at $x = 8\pi$ (line source position), $x = 9.5\pi$, $x = 11\pi$ and dashed line represents the y location of the line source

could be the fact that all quantities plotted shows no disturbances on the opposite side of the channel, thus falling back to the case in which the wire is not present.

Chapter 7

Conclusion

The aim of the thesis was the development of a new numerical code to study and understand problems related to hot wire anemometer measurements. The obstacles faced by experimentalists are related to the probe interaction with the wall and the spatial resolution affecting measurements as the Reynolds number increases to the regimes of practical interest. To do so, Direct Numerical Simulation were solved using a spectral element code. The advantage of such numerical scheme is the highly accurate solutions obtained in term of precision and resolution.

Starting from results obtained by Kasagi, [7], and the one by Kim & Moin [9], we start our validation process from a Channel flow at $Re_\tau = 180$ introducing passive scalar with a volume forcing term. Our addition was implementing a line source of heat represented by two exponential, mimicking the presence of a heat source in a spectral domain. Finally, combining both forcing terms we effectively introduced the "hot-wire" inside our domain keeping the Re_τ fixed throughout the entire validation process.

The most challenging part of the work was the combination of the two forcing terms, where the discontinuity represented by the line source and the volume heating hardly coexists. The line source of heat represents a strong discontinuity inside our domain while to the volume heating tends to fix the heat inside the channel at a constant value.

Performing such simulation, even if the computational burden was quite

high, allowed us to obtain a new data-set of information that could help us understanding and hopefully solve some open questions related to hot-wire anemometer interaction with the wall or filtering issues.

7.1 Future works

The present thesis opens a new path where direct numerical simulation with passive scalar could help us in understanding the interaction between turbulent flows and hot wire anemometer. The natural next step of this work would be the spectral analysis as well as the filtering both in space and time. Thanks to this new data-set one could compare data obtained from simulations with experimental studies carried out in other facilities.

Moreover the model could be improved by implementing not only the constant current anemometer as we did but also the constant temperature anemometer, one of the most used sensor in the last decades, allowing the comparison with a much broader set of experimental studies.

Finally, thanks to higher computing power achieved during these last years, it is possible to achieve higher and higher Reynolds number, obtaining resolution level that experimental studies can hardly obtain.

Acknowledgement

First of all I would like to thanks Professor Gabriele Bellani that give me the possibility to perform my thesis at KTH and for supporting me with every informations, from Fluid dynamics problems to Whatever needed. I would like to thank Professor Philipp Schlatter for inspiring and helping me whenever needed. Thanks to Professor Ramis Örlü for introducing me to the world of hot wire and in general to the aerodynamic.

Vorrei inoltre ringraziare i dottorandi Pierluigi Morra e Miguel Beneitez per tutto il supporto riguardante Simson, la vostra conoscenza è stata estremamente preziosa; anche fuori dalle mura universitarie. Un grazie a tutti coloro che mi hanno accompagnato durante la mia esperienza in Svezia: Franscesco, Stefano, Valerio e Gabriele per tutte le serate e non passate insieme

Inoltre Vorrei Ringraziare tutti i miei colleghi che mi hanno accompagnato in questi anni e che in questo giorno stanno condividendo con me la felicità nel concludere questo percorso.

Infine, vorrei ringraziare mia sorella e la mia famiglia per non aver mai smesso di credere in me e per avermi sempre appoggiato in ogni scelta fatta, senza di voi tutto questo non sarebbe possibile, Grazie.

Bibliography

[1] Universita D I Bologna. "Turbulent Pipe Flow - High Resolution Measurements in CICLoPE". In: (2017).

[2] Mattias Chevalier et al. *Simson User Guide*. 2007, pp. 1–100. ISBN: 9789171788382.

[3] G Comte-Bellot. "Hot-Wire Anemometry". In: *Annual Review of Fluid Mechanics* 8.1 (1976), pp. 209–231. DOI: 10.1146/annurev.fl.08.010176.001233.

[4] Hugh L Dryden et al. "Measurements of intensity and scale of wind-tunnel turbulence and their relation to the critical Reynolds number of spheres". In: (1937).

[5] N. Hutchins et al. "A direct measure of the frequency response of hot-wire anemometers: temporal resolution issues in wall-bounded turbulence". In: *Experiments in Fluids* 56.1 (2015). ISSN: 07234864. DOI: 10.1007/s00348-014-1856-8.

[6] Arne V Johansson and P Henrik Alfredsson. "Effects of imperfect spatial resolution on measurements of wall-bounded turbulentbx shear flows". In: *Journal of Fluid Mechanics* 137 (1983), pp. 409–421.

[7] N. Kasagi, Y. Tomita, and A. Kuroda. "Direct Numerical Simulation of Passive Scalar Field in a Turbulent Channel Flow". In: *Journal of Heat Transfer* 114.3 (1992), p. 598. ISSN: 00221481. DOI: 10.1115/1.2911323.

[8] John Kim and Parviz Moin. "Transport of passive scalars in a turbulent channel flow". In: *Turbulent Shear Flows 6*. Springer, 1989, pp. 85–96.

[9] John Kim, Parviz Moin, and Robert Moser. "Turbulence statistics in fully developed channel flow at low Reynolds number". In: *Journal of fluid mechanics* 177 (1987), pp. 133–166.

[10] Parviz Moin and Krishnan Mahesh. "Direct numerical simulation: a tool in turbulence research". In: *Annual review of fluid mechanics* 30.1 (1998), pp. 539–578.

[11] Ramis Örlü and P. Henrik Alfredsson. "On spatial resolution issues related to time-averaged quantities using hot-wire anemometry". In: *Experiments in Fluids* 49.1 (2010), pp. 101–110. ISSN: 07234864. DOI: 10.1007/s00348-009-0808-1.

[12] Ramis Örlü et al. "Thermal anemomentry". In: *Experimental Aerodynamics (ed. S. Discetti & A. Ianiro)* (2017), pp. 257–303.

[13] Stephen B. Pope. *Turbulent Flows*. Cambridge University press, 2000. ISBN: 9781139643351.

[14] Osborne Reynolds. "XXIX. An experimental investigation of the circumstances which determine whether the motion of water shall be direct or sinuous, and of the law of resistance in parallel channels". In: *Philosophical Transactions of the Royal society of London* 174 (1883), pp. 935–982.

[15] Antonio Segalini et al. "A method to estimate turbulence intensity and transverse Taylor microscale in turbulent flows from spatially averaged hot-wire data". In: *Experiments in Fluids* 51.3 (2011), pp. 693–700. ISSN: 07234864. DOI: 10.1007/s00348-011-1088-0.

List of Symbols

u	Fluctuation of the velocity
α_0	Resistivity coefficient of the reference material
δ	Channel heigth
δ_ν	Viscous legth scale
ϵ	Mean dissipation rate of energy
η	Kolmogorov scale
Γ	Diffusivity
Λ_l	Integral legth scale
Λ_t	Integral time scale
$\langle U \rangle$	Mean of the velocity
μ	Kinematic viscosity
ν	Dynamic viscosity
ω	Span wise component of the velocty
Ω_k	Angular velocity
ϕ	Passive scalar
π	Pi

ρ	Air density
σ_u	Standard deviation
τ_η	Kolmogorov time scale
τ_w	Wall friction
$\mathbf{f}$	External forces
$\mathbf{t}$	Body forces
θ	Passive scalar
A_ω	Convective heat transfer coefficient
a_T	Over heat ratio
b	Channel depth
D	Wire diameter
E	Voltage drop
e	Internal energy
F_i	i-th component of the flatness
h	Forced convection coefficient
h_ω	Angular velocity term
h_v	Body forces term
I	Current intensity
L	Channel length
L^+	Filtering legth scale
L_ω	Wire length
m	Mass

N_i	i-th component of the spectral modes
Nu	Nusselt number
P	Power
p	Pressure
Pe	Peclet number
Pr	Prandtl number
q	Heat
R_0	Resistance of the reference material
R_ω	Resistance of the hot wire
Re	Reynolds number
Re_τ	Friction Reynolds number
Re_b	Reynolds number normalized with bulk velocity
Re_{cl}	Reynolds number normalized with center line velocity
rms	Root Mean Square
S	Material Surface
S_i	i-th component of the skewness
T	Temperature
t	Time
T^*	Non dimensional temperature
T^+	Viscous temperature
T_0	Ambient temperature
T_ω	Temperature of the wire

T_τ	Friction temperature
U	Velocity vector
u^+	Velocity in wall units
u_η	Kolmogorov length scale
u_τ	Friction velocity
u_i	i-th component of the velocity
V	Material Volume
v	Wall normal component of the velocity
y^+	Channel distance in wall units
A	King's law coefficient
B	King's law coefficient
CDF	Cumulative Distribution Function
n	King's law coefficient
PDF	Probability Density Function